NASA CONTRACTOR REPORT

NASA CR-1167

NASA CR-1167

TRANSISTOR DESIGN EFFECTS ON RADIATION RESISTANCE

by C. C. Berggren and V. R. Honnold

Prepared by
HUGHES AIRCRAFT COMPANY
Fullerton, Calif.
for Langley Research Center

NATIONAL AERONAUTICS AND SPACE ADMINISTRATION • WASHINGTON, D. C. • SEPTEMBER 1968

NASA CR-1167

TRANSISTOR DESIGN EFFECTS ON RADIATION RESISTANCE

By C. C. Berggren and V. R. Honnold

Prepared under Contract No. NAS 1-6954 by
HUGHES AIRCRAFT COMPANY
Fullerton, Calif.

for Langley Research Center

NATIONAL AERONAUTICS AND SPACE ADMINISTRATION

For sale by the Clearinghouse for Federal Scientific and Technical Information
Springfield, Virginia 22151 – CFSTI price $3.00

TRANSISTOR DESIGN EFFECTS ON RADIATION RESISTANCE

By C. C. Berggren and V. R. Honnold

Hughes Aircraft Company
Hughes-Fullerton

SUMMARY

Analytical expressions relating transistor design parameters to radiation induced gain degradation have been developed. Emitter efficiency and base transport injection level effects have received prime consideration. Several statistically designed experiments, which employed custom designed planar transistor variations, were conducted to evaluate the theoretical conclusions.

The need for accurate profile information, to correlate with radiation induced gain degradation, is established. Shallow junctions and low base doping are shown to contribute significantly to radiation resistance.

CONTENTS

	PAGE
SUMMARY	iii
TABLE OF CONTENTS	v
LIST OF FIGURES	vi
LIST OF TABLES	viii
INTRODUCTION	1
THEORETICAL ANALYSIS	2
General Introduction	2
Double Diffused Transistor Structure	4
Space Charge Region Volume Recombination	9
Surface Recombination	9
Base Transport	11
Emitter Efficiency	21
Composite Variation of Radiation Sensitivity with Injection Level	30
EXPERIMENTAL PROCEDURE	35
Transistor Fabrication	35
Data Acquisition	37
Statistics	40
Device Irradiations	41
Electron Irradiation	42
Proton Irradiation	42
EXPERIMENTAL DATA AND COMPARISON WITH THEORY	46
Comparison of Mesa and Planar Processed Transistor Types	46
Variations in Emitter to Base Doping Ratio	51
Double Diffused Base	62
Factorial Designed Experiment	65
Design Verification	72
CONCLUSIONS	77
APPENDIX	79
Minority Carrier Distribution in Emitter Region	79
Proton Irradiation of Insulated Gate Tetrode	82
REFERENCES	89

LIST OF FIGURES

FIGURE	TITLE	PAGE
1	Variation in Common Emitter Current Gain with Emitter Current	3
2	Base Current Components	5
3	Doping Profile for Double Diffused Transistor	7
4	Profile in the Region of the Emitter Base Junction	8
5	Effects of Surface Recombination Component Upon Low Current Gain	10
6	Dependence of Injection Level Function upon Doping Profile	18
7	Coordinate System for Calculation of Emitter Efficiency	24
8	Analysis of Contributions to Reciprocal Gain	34
9	Contact Configuration for Planar Transistor Design Variations	36
10	Essentials of Measurement Circuit	39
11	Automatic Transistor Positioner Used For Electron Irradiations	43
12	Proton Beam Dosimetry	45
13	Radiation Induced Changes in Common Base Current Gain	49
14	Radiation Induced Changes in Common Base Current Gain	50
15	Radiation Induced Changes in I_{CBO}	52
16	Radiation Induced Changes in Reciprocal Gain	54
17A	Gain Characteristic for Irradiated Device No. 8	55
17B	Gain Characteristic for Irradiated Device No. 3	56
18	Injection Level Effects on Degradation in Reciprocal Gain	58
19	Double Diffused Base Transistor	63

FIGURE	TITLE	PAGE
20	Doping Profile and Effect Upon Minority Carrier Diffusion	63
21	Relative Rate of Change of $1/\beta$ for Variations of Double Diffused Base Transistors	64
22	Base Doping Profiles from Factorial Experiment	70
23	Transistor Doping Profile for Design Verification	73
24	Radiation Induced Changes in Reciprocal Gain for Groups 5,16,9 and the Radiation Resistant Prototype	74
25	Comparison of Prototype and Selected Variations from Factorial Experiment. Injection Level Effects on Reciprocal Gain Degradation	75
A1	Cross Section of Insulated Gate Tetrode	83
A2	Radiation Induced Changes in MOS Tetrode Transfer Characteristics	85
A3	Radiation Induced Changes in MOS Tetrode Transfer Characteristics	86
A4	Radiation Induced Changes in Drain Current Characteristic	87

LIST OF TABLES

	TITLE	PAGE
1.	Contributions to Slope of Reciprocal Gain	33
2.	Design Parameters for Emitter and Base Doping Ratio Variations	53
3.	Relative Radiation Sensitivity for Doping Ratio Variations	57
4.	Summary of Injection Level Data	61
5.	Design Parameters for Factorial Experiment	66
6.	Order of Decreasing Radiation Sensitivity of Sixteen Design Variations Under Electron Irradiation	67
7.	Order of Decreasing Radiation Sensitivity of Sixteen Design Variations Under Proton Irradiation	68
8.	Pre-Irradiation Test Data for Radiation Resistant Prototype and Representative Devices from Factorial Experiment	76

INTRODUCTION

A program of transistor design effects upon radiation sensitivity of planar processed bipolar transistors has been conducted. Design equations which incorporate profile parameters, minority carrier lifetime and injection level into expressions for base transport and emitter efficiency are developed.

A series of statistically designed experiments, with included profile and doping variations, were conducted. Design variables were mesa or planar structure, surface oxide, emitter and base doping concentrations, collector material, junction depth, gold doping and incorporation of a base region enhancement diffusion.

All transistors were irradiated with 10MeV electrons at the Hughes Research Linac. Common base current gain was measured as a function of emitter current at approximately seven fluence levels up to $5 \cdot 10^{14}$ electrons/cm^2. Sixteen design variations were irradiated at the University of Southern California 31McV proton LINAC to establish the general application of radiation resistant design for both electron and proton irradiation.

A final design variation, which extended those features most significant in establishing radiation resistance, was fabricated and shown to be superior to the previous variations.

Additionally, a MOS field effect majority carrier device, a two gate MOS tetrode developed at Hughes Newport, was irradiated at the 31MeV proton facility. Degradation in transconductance, g_m, was observed for operation in both triode and pentode modes of operation. Gain degradation was explained by introduction of positive space charge in the oxide material.

THEORETICAL ANALYSIS

General Introduction

The analysis of transistor design effects on radiation resistance is approached, in what follows, in two complementary ways. These are: a theoretical analysis of several components of transistor current flow, with modifications to include radiation induced transistor gain degradation; and, an empirical investigation of design effects on experimentally determined radiation sensitivity.

The first and primary point to be noted is that, just as the parameter which determines common emitter current gain, β, is a function of the operating point, the factor which determines the sensitivity to high energy radiation is also a function of the operating point. Consider a β vs I_E plot, typical of devices presented in later sections, as shown in Figure 1. At very low emitter currents ($< 10\ \mu A$) the controlling parameter may be the recombination currents in the emitter base space charge region in the bulk or at the surface (ref. 1). As the current increases the significance of these components decrease as compared to base region surface recombination and volume recombination. At the peak of the curve the recombination in the emitter volume (emitter efficiency component) takes over and the gain then decreases with emitter current.

A convienent way to consider these separate contributions to current gain is to form the expression for reciprocal gain.

$$1 / \beta = I_B / I_C$$

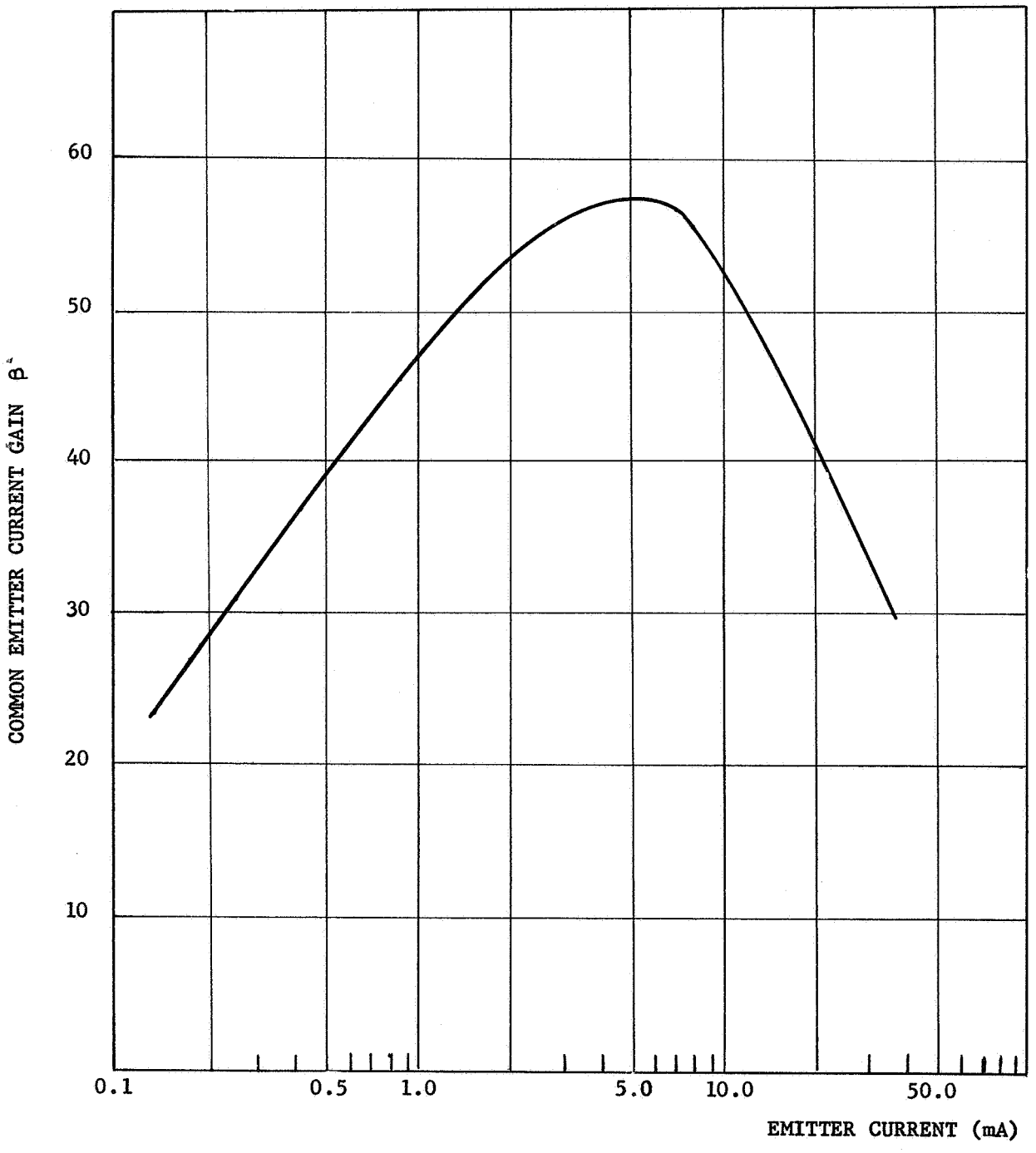

FIGURE 1 - VARIATION IN COMMON EMITTER CURRENT GAIN WITH EMITTER CURRENT

The base current I_B is made up of several components,

$$I_B = I_{VR} + I_S + I_{ER} + I_{GR} \quad ,$$

where I_{VR} = base region volume recombination,
I_S = base region surface recombination,
I_{ER} = emitter region volume recombination, and
I_{GR} = depletion region volume recombination.

These current components are illustrated in Figure 2.

For useful values of the current gain we may replace I_C by I_E to obtain

$$1 / \beta = I_{VR} / I_E + I_S / I_E + I_{ER} / I_E + I_{GR} / I_E \qquad (2)$$

Equation 2 forms the basis for a discussion of the various effects which act to control current gain in the various regions of low to high injection level. In the following sections we will examine these terms with particular emphasis on base transport and emitter efficiency.

Double Diffused Transistor Structure

The transistor structures to be considered in this report are produced by the double diffused planar process. Starting material in each case is an epitaxial layer of .5 to 2 Ω-cm n-type silicon on a low resistivity wafer. Both base and emitter diffusion steps are

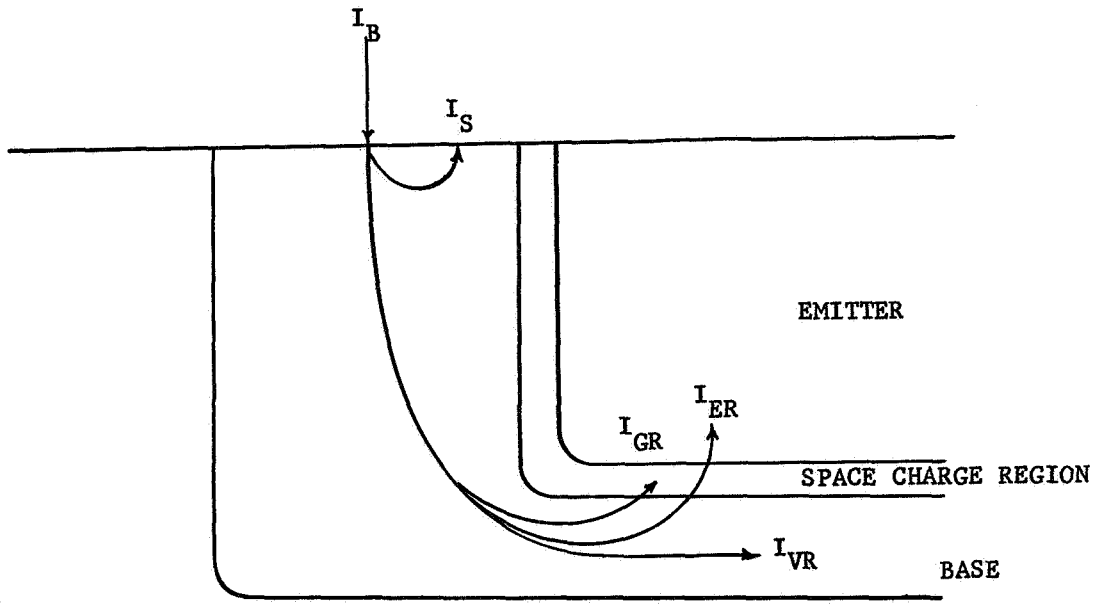

FIGURE 2 - BASE CURRENT COMPONENTS

composed of a deposit and drive cycle. This process sequence, diffusion from a fixed amount of material on the surface (the deposit step), results in a gaussian doping profile for both emitter and base doping impurities. The net doping concentration is the sum of the two gaussian terms plus a uniform background term

$$N = + N_{ES} \exp (x^2 / k_1) - N_{BS} \exp (x^2 / k_2) + N_C \qquad (3)$$

where N_{ES} = emitter surface concentration,
N_{BS} = base surface concentration,
N_C = collector doping concentration, and
x = distance from emitter surface.
k_1 & k_2 = constants relating to junction depth.

Direct determinations of the emitter and base junction depths are obtained from angle cross sections of the transistor. The resistivity (ohms per square) of the base and emitter diffusions are determined by four-point probe measurements. With this data the surface concentration may be determined with the aid of Irvin's (ref. 2) profile curves. The values of k_1 and k_2 are determined by evaluating Equation 3 with $N = 0$ at the emitter (x_{je}) and base (x_{jb}) junction depths.

The results of such analysis for a typical transistor profile are presented in Figure 3 to illustrate several important parameters referred to in subsequent sections. The features to be noted are the steep gradients in doping present in the emitter and base region. In Figure 4 a more detailed plot of the doping concentration in the region of the emitter base junction is shown to illustrate the linear grade approximation made in the depletion region.

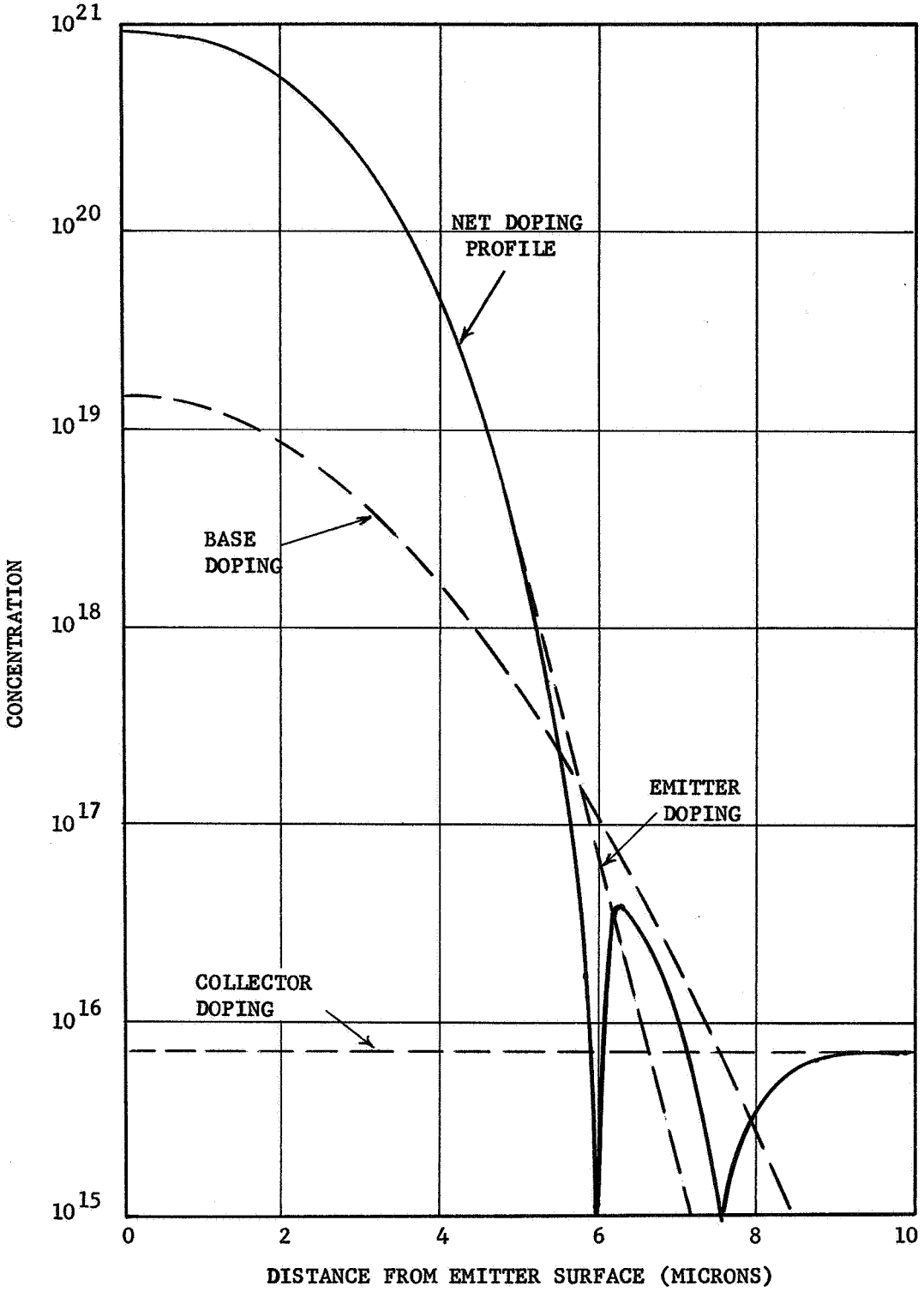

FIGURE 3 - DOPING PROFILE FOR DOUBLE DIFFUSED TRANSISTOR

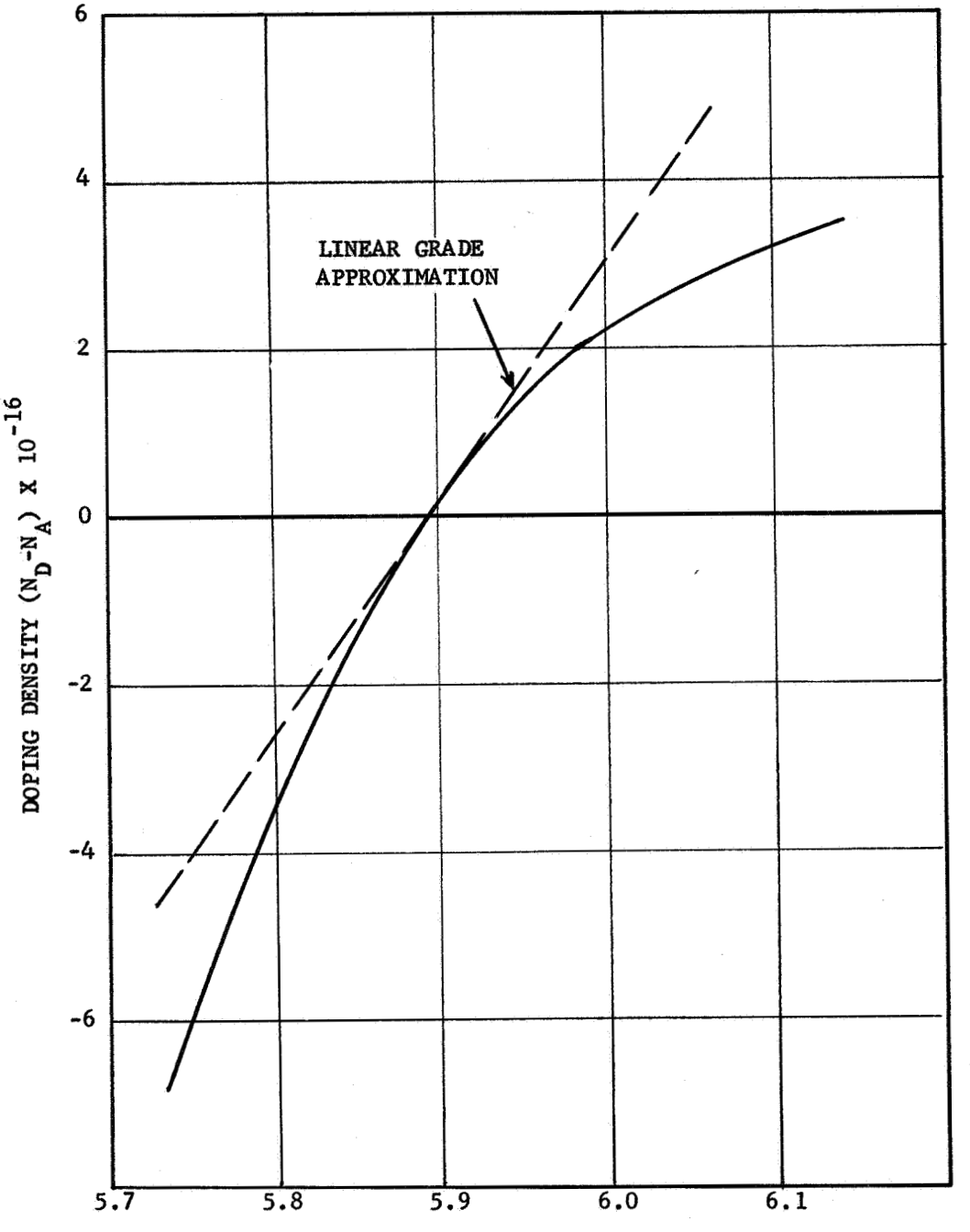

FIGURE 4 - PROFILE IN THE REGION OF THE EMITTER BASE JUNCTION

Space Charge Region Volume Recombination

For several reasons the third term in Equation 2, the expression for recombination in the emitter depletion region, has not been investigated in the current report. The importance of this term decreases with injection level (ref. 1) and the injection level considered in this report, 200 μA to 50 mA in a 4.5 mil emitter, is considered to lie above the range of importance for this term. The circular geometry employed minimizes the edge to area ratio and thus the relative importance of edge injected current components. Additionally, the data has been explained adequately by the remaining terms for the design variations considered in this study.

Surface Recombination

The importance of surface recombination in determining the low current transistor gain has been demonstrated, in related programs at Hughes Aircraft Company, by comparison of β vs I_E curves for devices which have received special annealing treatments to those for devices with standard processing. The effect of the surface annealing is illustrated in Figure 5. It should be noted that the low current β was increased to make β nearly independent of operating point up to the point where the peak of the β vs I_E curve occurs for the untreated device. The remaining portion of emitter current dependent β may be contributed by base transport (discussed in the next section) and the remainder by surface recombination effects. Mitchell (ref. 1) observes that a change in surface recombination velocity of nearly an order of magnitude will occur at ionizing dose levels below those associated with bulk damage. Such changes in surface recombination velocity tend to saturate with dose. This behavior is more obvious at low current levels where such dose dependence may be distinguished from the linear dependence of reciprocal lifetime upon fluence. Such effects will be noted when experimental data is presented in later sections.

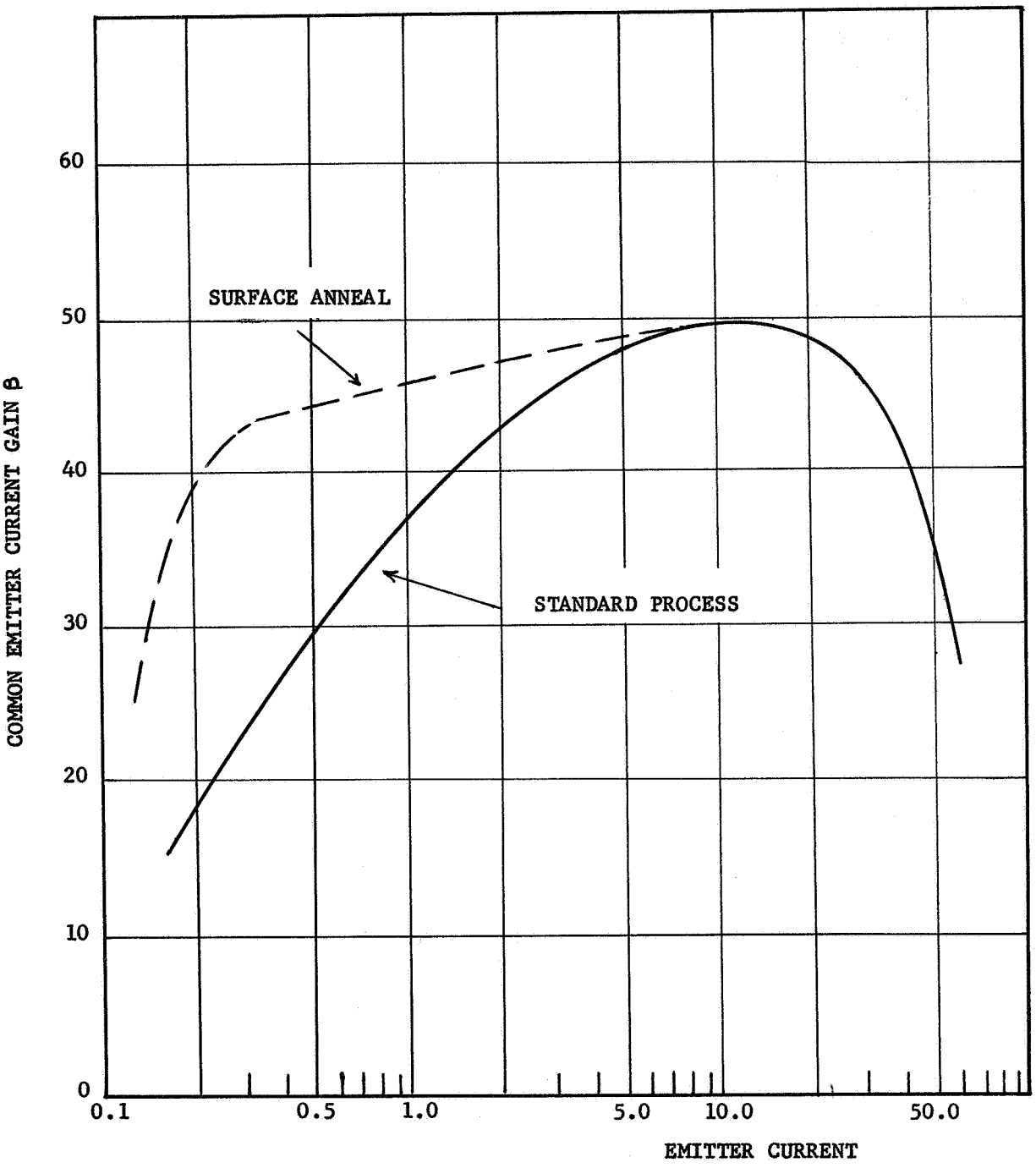

FIGURE 5 - EFFECTS OF SURFACE RECOMBINATION COMPONENT UPON LOW CURRENT GAIN

Base Transport

The base transport factor is equal to one minus the probability of volume recombination for a minority carrier injected from the emitter into the base region of the transistor. For simple one-dimensional current gain analysis and the case of uniform base doping the base transport factor is

$$\beta^* = 1 - W^2 / (2 D \tau) \qquad (4)$$

For application to the class of double diffused transistors, operated over the full range of emitter currents for which the device possesses a useful gain, this expression must be generalized. The result of such a generalization will be the inclusion of electric fields due to the doping gradients present in the double diffused structure as well as the electric field due to high injection levels. Additionally, the minority carrier lifetime must be modified in accordance with Shockley-Read theory to include its dependence upon injection level.

Modifications to include high level injection have been developed by Honnold, et al, (ref. 3) for the case of dc current gain and Messenger (ref. 4) for ac current gain. In each case, the validity was restricted to high injection levels and uniform base doping.

The generalization to include details of base doping profile will be restricted to a consideration of the exponential doping profile. The exponential doping profile is a consequence of the assumption of constant electric field. This approximation permits considerable simplification in this and the following section on emitter efficiency

and at the same time possesses close agreement with details of the double diffused structure, as both gaussian and error functions are approximately exponential sufficiently far below the surface.

For an exponentially doped base, the impurity profile is of the form

$$N_A = N_e \exp (- x / x_e) \qquad (5)$$

where N_A = net acceptor doping,
N_e = concentration at the base edge of the emitter base depletion region,
x_e = characteristic length in doping profile, and
x = distance from base edge of emitter base depletion region.

In this section the coordinates for the profile description will be the net acceptor density as a function of distance from the emitter base depletion region (the edge being $x = 0$).

When the injected minority carrier density is low, the built-in electric field may be obtained from the condition of zero majority carrier current.

$$0 = q \mu E p - q D (dp / dx) \qquad (6)$$

with the hole density equal to the net acceptor density

$$p = N_e \exp (- x / x_e) \quad . \tag{7}$$

Combining Equations 6 and 7 gives,

$$E = - (kT / q) / x_e \quad . \tag{8}$$

If we define a base field parameter η by $\eta = W / x_e$, Equations 5 and 8 may be rewritten as

$$N_A = N_e \exp (- \eta x / W) \tag{9}$$

and

$$E = - (kT / qW) \eta \quad . \tag{10}$$

The total current due to carriers lost to volume recombination is given by

$$I_{VR} = q A \int_o^W (n(x) / \tau(x)) \; d x \tag{11}$$

where A = emitter area,

$n(x)$ = injected minority carrier density,

$\tau(x)$ = minority carrier lifetime.

The Shockley-Read correction for injection level dependent lifetime is given by (ref. 5)

$$1 / \tau = (1 + cn) / [(1 + an) \tau_o] \quad (12)$$

where c = $1 / N$,

a = $\tau_\infty / (\tau_o N)$, and

N = doping density.

In Equation 12 both n and N are functions of distance from the edge of the emitter base depletion region. τ_∞ is the high injection level minority carrier lifetime given by Shockley-Read theory.

The remaining term to be expressed is the contribution of injected minority carriers to base electric field. This is accomplished by requiring charge neutrality in addition to the assumption of zero majority carrier current

$$p = N_A + n \quad (13)$$

and

$$dp / d x = d N_A / dx + dn / dx \ . \quad (14)$$

Combine Equations 6, 13 and 14 to obtain,

$$E = (kT / q) \left[d N_A / dx + dn / dx \right] / (N_A + n) \quad . \quad (15)$$

To completely specify the distribution of injected minority carriers we may consider the emitter current to be a constant equal to the collector current, this assumption is valid for transistors which possess a useful current gain. The emitter current is given by

$$I_E = q \mu A E n + q D A (dn / dx) \quad (16)$$

Combining Equations 15 and 16, and making use of $D = (k T / q) \mu$ gives,

$$I_E = qDA \left\{ n \left[d N_A / dx + dn / dx \right] / (n + N_A) + dn / dx \right\} \quad . \quad (17)$$

Equations 11 and 12 may now be combined, finally, to give the volume recombination current,

$$I_{VR} = q A \int_o^W n (1 + cn) / \left[(1 + an) \tau_o \right] dx \quad . \quad (18)$$

Before proceeding to a calculation of the dependence of base transport on emitter current, it is desirable to introduce several dimensionless variables:

$$v = n / N_e \quad ,$$

$$y = x / W \quad , \text{ and} \tag{19}$$

$$Z = I_E W / (q D N_e A) \quad .$$

Equation 17 becomes, for N_A given by Equation 9

$$Z = \frac{- \eta v \exp (- \eta y) + \left[2 v + \exp (- \eta y) \right] \quad dv / dy}{2 v + \exp (- \eta y)} \tag{20}$$

Equation 18 can be rewritten as

$$I_{VR} = (qAN_e W / \tau_o) \int_o^1 \frac{v \left[1 + v \exp (\eta y) \right]}{\left[1 + v (\tau_\infty / \tau_o) \exp (\eta y) \right]} \, dy \tag{21}$$

To calculate the dependence of base transport upon emitter current, the following procedure is required.

1. Select the appropriate profile parameters; W, η, N_e .

2. Select the operating emitter current

3. From Equation 20 solve for v as a function y (note that v = 0 at y = 1 which serves as a starting point for numerical calculations)

4. With v determined in Step 3 perform the required integration of Equation 21 to obtain I_{VR}.

5. Base transport factor is defined as

$$\beta^* = 1 - I_{VR} / I_E \tag{22}$$

Recalling the expression for base transport given in Equation 4 we may define a function $H(Z)$ which produces the required generalization developed in this section.

$$\beta^* = 1 - W^2 / (2 D \tau_o) \; H(Z) \quad . \tag{23}$$

From Equations 19, 21 and 22 the function $H(Z)$ is evidently,

$$H(Z) = - (2/Z) \int_o^1 \frac{v \left[1 + v \exp (\eta y) \right] dy}{\left[1 + v (\tau_\infty / \tau_o) \exp (\eta y) \right]} \tag{24}$$

The minus sign is due to Z, I_E, and I_{VR} being negative.

A plot of the function $H(Z)$ vs Z is shown in Figure 6 for a particular choice of τ_∞ / τ_o with η as a parameter for the family of solutions.

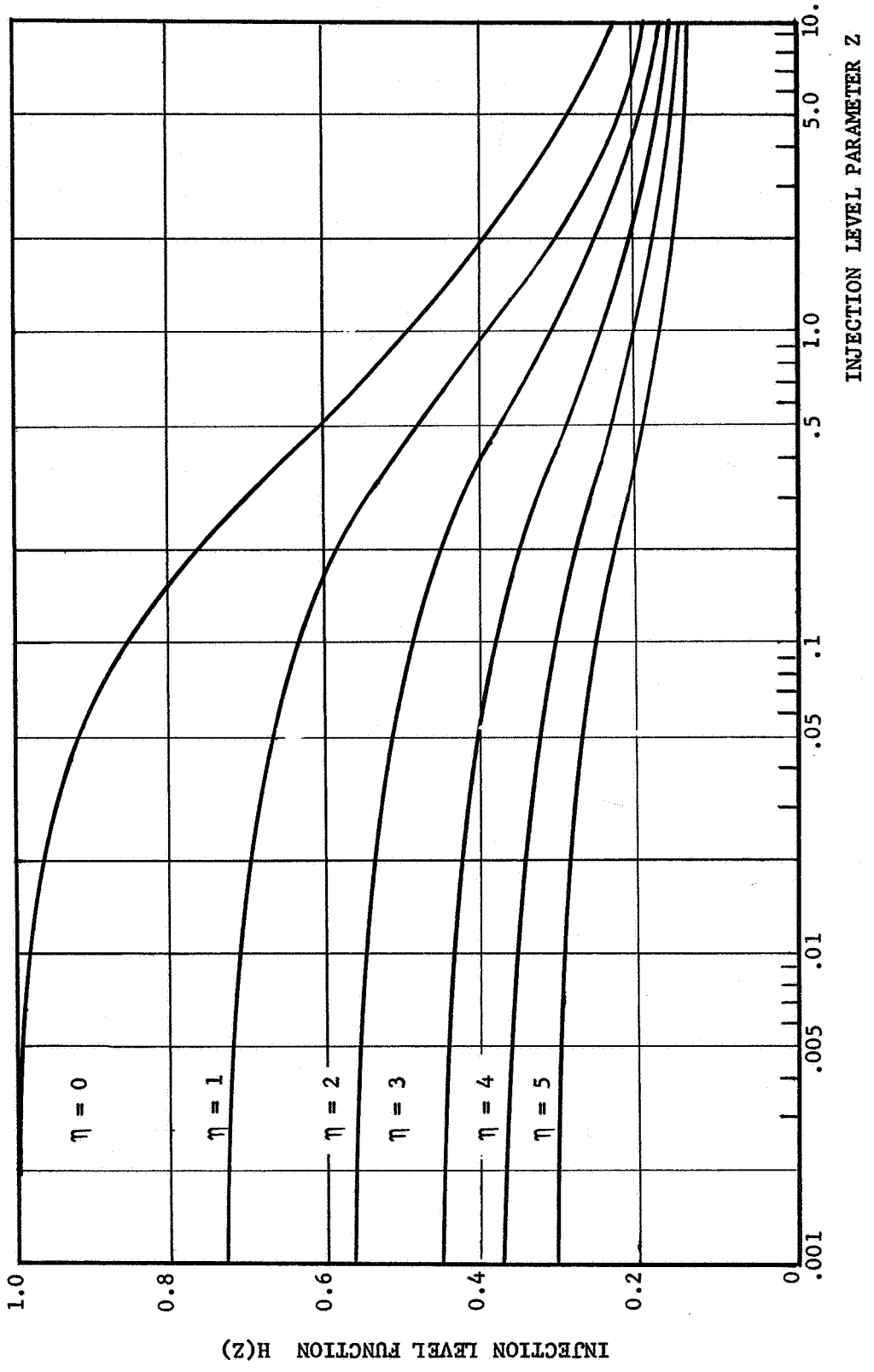

FIGURE 6 - DEPENDENCE OF INJECTION LEVEL FUNCTION ON DOPING PROFILE

Useful analytic expressions may be derived for both the low and high level injection limits of Equation 24. In the low injection level limit, the base region electric field is that due to the doping profile above, and Equation 15 reduces to:

$$E = (kT / q) \left[dN_A / dx \right] / N_A \tag{25}$$

Equation 17, the expression for injected emitter current, reduces to

$$I_E = qDA \left[(n / N_A) \, dN_A / dx + dn / dx \right] . \tag{26}$$

N_A given by Equation 9 and I_E are assumed constant, Equation 26 is a linear first order equation which determines $n(x)$. The solution in terms of the dimensionless variables defined by Equation 19 is

$$v = (Z / \eta) \left\{ \exp \left[\eta \, (y - 1) \right] - 1 \right\} . \tag{27}$$

For low injection level $v \ll 1$ and Equation 24 becomes

$$H(Z) = - (2 / Z) \int_0^1 v \, dy . \tag{28}$$

Equations 27 and 28 can be combined to obtain

$$H(Z) = -(2/\eta)\int_0^1 \left\{ \exp\left[\eta(y-1)\right] - 1 \right\} dy \qquad (29)$$

$$= -(2/\eta)\left\{ 1/\eta - e^{-\eta}/\eta - 1 \right\} ,$$

which represents the desired analytic expression for dependence of base transport upon base profile in the limit of low injection.

For high injection levels ($n > N_A$), the built-in fields are unimportant and the distribution of injected carriers is linear. Equation 17 reduces to

$$I_E = 2qDA \; dn / dx \; , \qquad (30)$$

which may be solved in terms of the dimensionless parameters to obtain

$$v = (Z/2)(y-1) \; . \qquad (31)$$

For high level injection $v \gg 1$ and Equation 24 reduces to

$$H(Z) = -(2/Z)\int_0^1 (\tau_o/\tau_\infty)\, v\, dy \qquad (32)$$

Upon combining Equations 31 and 32 the function H(Z) becomes

$$H(Z) = -(\tau_o/\tau_\infty)\int_0^1 (y-1)\, dy \quad ,$$

$$= (\tau_o/\tau_\infty)/2 \quad , \qquad (33)$$

which is the desired analytic expression for base transport corrected for high injection level.

Emitter Efficiency

The emitter efficiency is defined as the ratio of minority carrier current injected into the base to the total current,

$$\gamma = I_n/(I_n + I_p) \qquad (34)$$

where I_n = electron current injected into base, and
I_p = hole current injected into emitter.

If we consider $\gamma \approx 1$, Equation 34 may be written as,

$$\gamma \simeq 1 - I_p / I_n \quad . \tag{35}$$

For uniformly doped emitter and base regions, γ , in terms of transistor design parameters, is (ref. 6)

$$\gamma = 1 - \rho_e W / \rho_b L_{pe} \quad , \tag{36}$$

where ρ_e and ρ_b are, respectively, emitter and base resistivities, W is the base width, and L_{pe} is the hole diffusion length in the emitter.

Klein (ref. 7) in an effort to make the expression for emitter efficiency more explicitly a function of doping profile, assumed a power law doping profile and solved the associated continuity equation. The resultant equation is of the class of Bessel equations and a closed form solution was obtained for the case of a integral power law. An important feature of this solution is that the ratio I_p / I_n is inversely proportional to minority carrier lifetime in the emitter. If this is the case, a change in β which follows the law of lifetime degradation will have two possible explanations, base transport or emitter efficiency (or a combination of the two which will later be shown to be a reasonable assumption).

If, instead of a power law doping profile, an exponential doping distribtuion is assumed the differential equation remains linear. For convenience, the emitter edge of the depletion region is taken as $x = 0$

with the positive x-axis extending towards the emitter surface as shown in Figure 7. The doping profile in the emitter region is of the form

$$N(x) = N_{es} \exp\left[- (x_{je} - x_{eb} - x) / x_e \right] \qquad (37)$$

where N_{es} = extrapolated surface concentration,
x_{je} = emitter junction depth,
x_{eb} = width of positive space charge layer,
x_e = characteristic length of exponential doping.

From the condition of zero majority carrier current we obtain the built-in electric field,

$$I_n = 0 = q \mu_n A E n + q A D_n dn / dx \ . \qquad (38)$$

With $n = N(x)$, low injection in emitter side of junction, and $(D / \mu) = k T / q$ we obtain

$$E = - (kT / q) d\left[\ln (N) \right] / dx \qquad (39)$$

which is

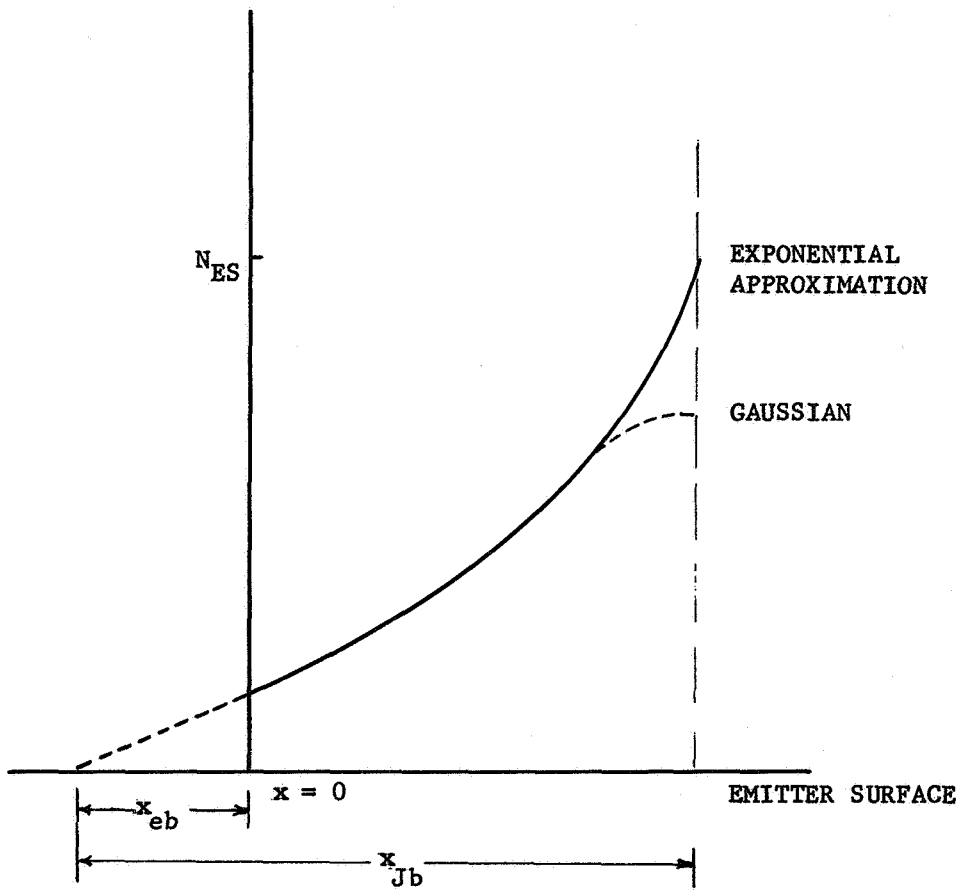

FIGURE 7 - COORDINATE SYSTEM FOR
CALCULATION OF EMITTER EFFICIENCY

$$E = - k T / q x_e = \text{constant} . \quad (40)$$

If a constant effective mobility and diffusion constant are assumed, the steady state minority carrier hole distribution in the emitter is governed by the diffusion equation in the form

$$D_p d^2p / dx^2 - \mu_p E dp / dx - p / \tau_p = 0 . \quad (41)$$

Substitute the expression for the electric field and make use of $\mu_p = q D_p / k T$ and $L_{pe}^2 = D_p \tau_p$ to obtain

$$d^2p / dx^2 + (1 / x_e) dp / dx - p / L^2_{pe} = 0 . \quad (42)$$

The solution of Equation 42 is of the form

$$p(x) = C_1 \exp (m_1 x) + C_2 \exp (m_2 x) \quad (43)$$

where

$$m_{1,2} = (1/2) \left[- 1 / x_e \pm (1 / x_e^2 + 4 / L^2_{pe})^{\frac{1}{2}} \right] . \quad (44)$$

The boundary conditions are

$$\begin{aligned} p &= p(0) \quad \text{at} \quad x = 0 \\ p &= 0 \quad \text{at} \quad x = x_{je} - x_{eb} \end{aligned} \tag{45}$$

In the Appendix it is shown that for typical values of the transistor parameters, Equation 43 reduces to

$$p(x) = p(0) \exp\left\{ -\left[1 + \left(1 + 4 x_e^2 / L_{pe}^2 \right)^{\frac{1}{2}} \right] x / 2x_e \right\} . \tag{46}$$

The current density is given by

$$J_p = q \mu E p - qDdp / dx \tag{47}$$

Substitution of Equations 40 and 46 into 47 and evaluating at $x = 0$ leads to,

$$J_p = \left[qD_p p(0) / 2x_e \right] \left[\left(1 + 4 x_e^2 / L_{pe}^2 \right)^{\frac{1}{2}} - 1 \right] . \tag{48}$$

For typical transistor profiles x_e is the order of 10^{-5} cm. Thus, if the emitter lifetime is of the order of tens of nanoseconds, Equation 48 reduces to

$$J_p = qD_p p(0) x_e / L^2_{pe} = qp(0) x_e / \tau_p \quad (49)$$

To form an expression for emitter efficiency, a relationship for total emitter current in terms of profile data is required. Since the base profile parameter, η, is equal to or greater than 3 for the typical planar structures, discussed in later sections, a good assumption is that the total emitter current is in the drift component at the emitter edge of the base. In this limit the emitter current density is given by

$$J_e = qD_n n (x_{be}) \eta / W \quad (50)$$

where x_{be} = distance to edge of depletion region in the base.

Substitution of Equations 49 and 50 into 35 yields

$$\gamma = 1 - (p(0) x_e W) / (D_n n (x_{be}) \eta \tau_p) . \quad (51)$$

The minority carrier concentrations in Equation 51 may be related to the doping densities just outside the depletion region at low injection levels by

$$p(0)\ N_D \quad = \quad n\ (\ x_{be}\ )\ \ N_A \quad . \tag{52}$$

With this substitution Equation 51 becomes,

$$\gamma \quad = \quad 1 - (\ x_e\ W\ N_A\ )\ /\ (\ D_n\ N_D\ \eta\ \tau_p\ ) \quad . \tag{53}$$

Equation 53 represents the desired expression for emitter efficiency which contains terms explicitly dependent upon the transistor profile, and may be compared with the constant doping case in Equation 36. An important feature, which is shown, is the inverse dependence upon lifetime. Such a result was obtained by Klein (ref. 7) for power law doping profiles. Physically, the inverse dependence on lifetime is due to forcing the minority carrier density to zero in a distance short compared to a diffusion length. In the base region, that condition is obtained as a result of the reversed bias collector junction. For the case considered by Klein, and for the development above, the important parameter is the strong diffusion opposing built-in field which is a general characteristic of double diffused transistors. A useful alternate expression is obtained by noting that N_D / x_e is equal to the linear grade constant (a) for the emitter base junction which may be determined from capacitance voltage measurements.

At high injection levels in the base (the higher emitter doping reduces the influence of carriers injected into the emitter) the expression for base current, Equation 50, is given by twice the low level diffusion component (ref. 6)

$$J_e = 2 q D_n n (x_{be}) / W \qquad (54)$$

Equation 52 which relates the minority carrier density to doping density is modified at high injection to include charge neutrality in the base by

$$p(0) N_D = n (x_{be}) \left[N_A + n (x_{be}) \right] . \qquad (55)$$

With Equations 54 and 55 the high injection level emitter efficiency is given by

$$\gamma = 1 - \frac{x_e W N_A}{2 D_n N_D \tau_p} \left[1 + n (x_{be}) / N_A \right] . \qquad (56)$$

At high injection levels the ratio of $n(x_{be}) / N_A$, from Equation 19, may be seen to equal $Z/2$. The emitter efficiency thus decreases with injection level as

$$\gamma = 1 - \frac{x_e W N_A}{2 D_n N_D \tau_p} (1 + Z / 2) \qquad (57)$$

which is valid for large values of Z to allow the approximation in Equation 54.

Equation 57 represents the desired high injection level expression for emitter efficiency with direct dependence on transistor profile parameters.

Composite Variation Of Radiation Sensitivity With Injection Level

In the preceding three sections (Surface Recombination, Base Transport. and Emitter Efficiency) the variation in reciprocal gain with injection level has been discussed. In this section the combined effects of surface recombination, base transport, and emitter efficiency are considered in a qualitative manner to illustrate the variation of reciprocal gain with radiation. Explicit use of design parameters in determining the contribution of base transport and emitter efficiency is possible through Equations 23 and 51 while the contribution of surface recombination is inferred from data such as that presented in later sections.

As a specific example, we will consider a transistor with emitter and base diffusion depths of 2.3 and 3.8 microns, respectively, and surface concentrations of 6.4×10^{20} cm^{-3} and 8.0×10^{17} cm^{-3}, respectively. These values correspond to device 1 of the factorial experiment discussed in a later section. Following the analysis outlined in the previous section, we arrive at the following profile parameters:

. Base Width	1.5 microns
. Base Concentration at Emitter Edge	3.0×10^{16} cm^{-3}
. Emitter Base Grade Constant	5.0×10^{21} cm^{-4}
. Effective Base Diffusion Constant	18 cm^2/sec
. Base Field Parameter	4.25

The contribution to the reciprocal gain of the base transport and emitter efficiency is obtained from

$$1 / \beta = 1 - \beta^* \gamma \qquad (58)$$

From Equations 28, 29 and 53, the reciprocal gain is, for low injection levels,

$$1 / \beta = W^2 / (\eta D \tau_n) + (W N_A) / (D_n a \eta \tau_p) \quad . \qquad (59)$$

At the high injection levels, Equations 23, 33 and 57 combine to produce

$$1 / \beta = \frac{W^2 (\tau_o / \tau_\infty)}{4 D \tau_n} + \frac{W N_A}{2 D_n a \tau_p} (1 + Z / 2) \qquad (60)$$

where $a = N_D / x_e$ has been substituted into both Equations 59 and 60.

The generalization of Equations 59 and 60 to include radiation effects follows directly from the expression for lifetime degradation,

$$1 / \tau = 1 / \tau_o + K \phi \quad , \qquad (61)$$

where ϕ is the exposure fluence (particles/cm^2).

When Equation 61 is substituted into Equations 59 and 60, assuming the damage constant, K, to be the same in the emitter and base region, the rate of change of reciprocal gain with flux is,

a. Low injection

$$d (1 / \beta) / d \phi = W^2 K / (\eta D_n) + (W N_A K) / (D_n a \eta) \quad (62)$$

b. High injection

$$d (1 / \beta) / d \phi = \frac{W^2 K (\tau_o / \tau_\infty)}{4 D_n} + \frac{W N_A K}{2 D_n a} (1 + Z / 2) \quad (63)$$

Evidently if $(\tau_o / \tau_\infty) < 4 / \eta$, the contribution of base transport to the slope of $1 / \beta$ vs flux decreases with emitter current to a fixed lower limit. The contribution of emitter efficiency is evidently a linearly increasing function of emitter current at the high level limit. With the previous numerical data for the design parameters, the contributions to the increase in reciprocal gain are presented in Table 1. As suggested in the General Introduction (of this section), the parameter which controls $d(1 / \beta) / d \phi$ is obviously a function of operating point. A qualitative composite of the contributions to reciprocal gain is presented in Figure 8. From examination of typical data, the saturating component, that assumed due to surface recombination, is most predominate at low currents. Although it was not possible to determine initial lifetimes to determine the breakdown of initial $1 / \beta$, values were assumed such that surface recombination was the predominate

TABLE 1-CONTRIBUTIONS TO SLOPE OF RECIPROCAL GAIN $\left(\frac{d\ 1/\beta}{d\ \phi} \right)$

	Low Injection ($Z \ll 1$)	High Injection ($Z = 10$, $\tau_o/\tau_\infty = 0.3$ *)
Base Transport ∓	2.94×10^{-10}	$.94 \times 10^{-10}$
Emitter Efficiency	1.18×10^{-11}	1.5×10^{-10}

∓ Normalized to unity damage constant

* Assumed value, typical of data presented by Curtis (ref. 8)

factor in low injection, β_o, while emitter efficiency controls high current initial β_o . Later examples of experimental data will illustrate such a decrease in the slope of $1 / \beta$ vs flux with emitter current followed by an increase with emitter current.

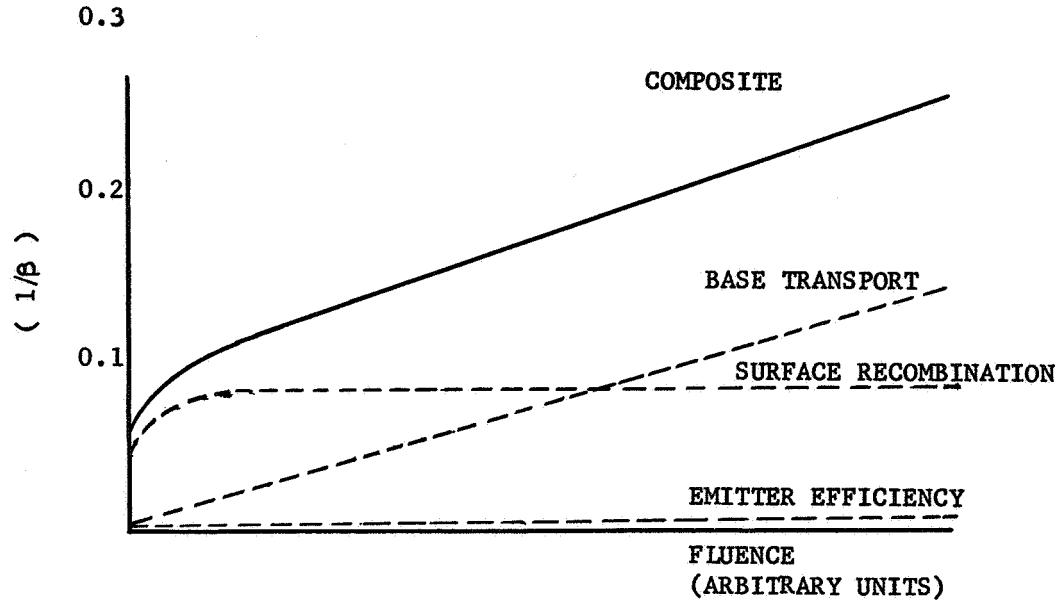

(a.) LOW INJECTION

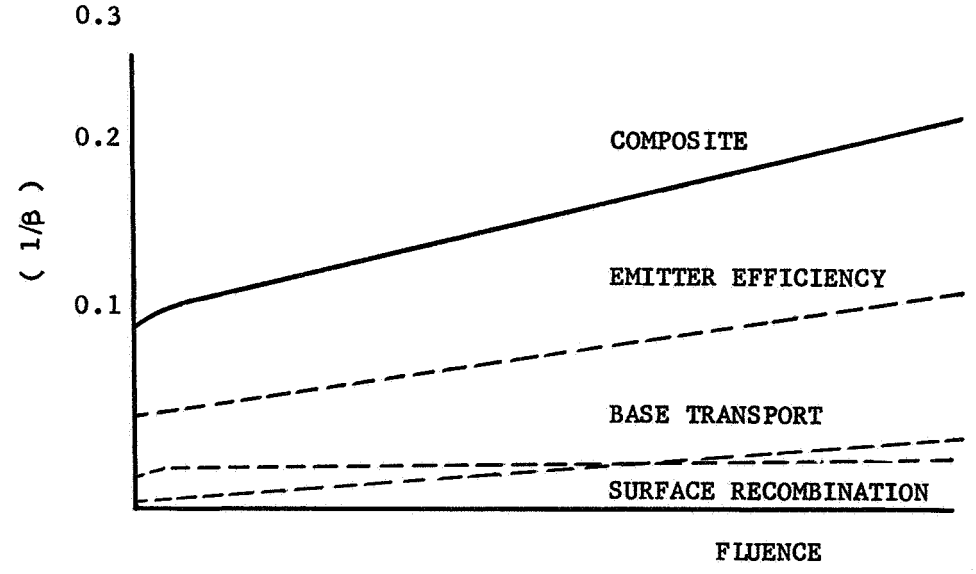

(b) HIGH INJECTION

FIGURE 8 - ANALYSIS OF CONTRIBUTIONS TO RECIPROCAL GAIN

EXPERIMENTAL PROCEDURE

Transistor Fabrication

The primary objective of the current program of design effects upon radiation resistance in the planar bipolar transistor is a determination of the effects of profile variations. The geometrical design selected, a mask set used in production of the 2N2484, is shown in Figure 9. The emitter and base diffusion diameters are 4.25 and 9.0 mils, respectively. In addition, special masks were produced for definition of the mesa region in the mesa-planar comparison experiment as well as special masks for making contact to the no-oxide variations in this same test.

In the evaluation of design effects, the present program has performed three preliminary experiments in which the effects of (1) mesa vs planar configuration with and without passivation oxide, (2) variations in emitter to base doping density ratio and, (3) inclusion of an enhanced base doping ring surrounding the emitter, were evaluated. Following these experiments a 2^4 factorial experiment was conducted in which four design parameters: junction depth, collector material, base doping, and gold doping were obtained for all combinations of each factor at two levels. The factor levels were selected to give a wide range in device design with the limitation that each design be a useful transistor.

Ideally, when a particular design variable such as base concentration is being varied, all other parameters such as base width, junction depth and emitter concentration should be held constant. This, however, is not possible without excessive trial runs to determine exact diffusion

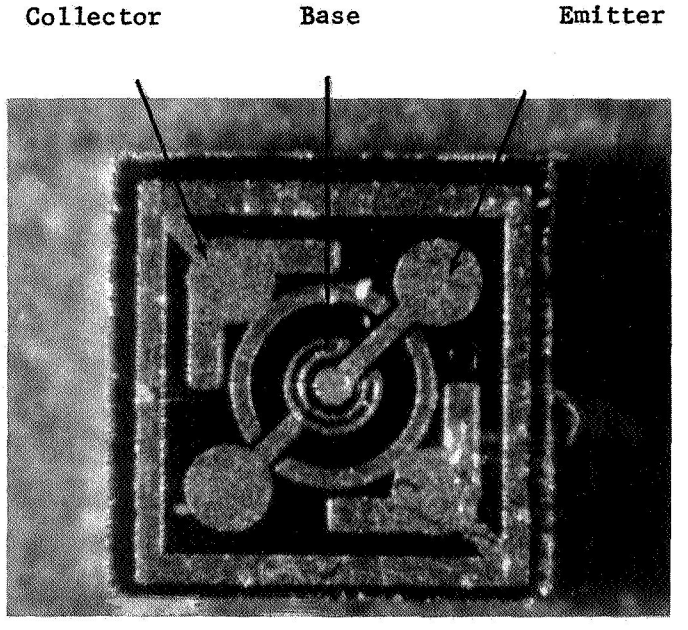

FIGURE 9 - CONTACT CONFIGURATION FOR
PLANAR TRANSISTOR DESIGN VARIATIONS

times and temperatures. To offset this problem a complete description of the transistor profile through angle cross sections and resistivity measurements was conducted. Additionally, careful records of the process steps were maintained to provide a basis for evaluating any unexpected results in the radiation testing. Although no attempt was made to stay within the specifications of a given transistor type, a complete set of electrical characteristics including BV_{CBO} , BV_{CEO} , BV_{EBO} , $V_{CE}(SAT)$, and h_{FE} were measured to select units for radiation testing. This electrical evaluation not only insures that the experimental devices are useful transistors, but permits a correlation of radiation sensitivity with electrical parameters and an evaluation of processing on electrical performance.

Data Acquisition

To relate to the theoretical analysis of the Theoretical Analysis section, the radiation sensitivity was characterized through a determination of the curve of reciprocal gain as a function of flux. In particular, as pointed out in the Composite Variation Of Radiation Sensitivity With Injection Level portion of the preceding section, it was necessary to obtain a family of curves for $1 / \beta$ as a function of flux with emitter current as a parameter to characterize the radiation sensitivity. In total, 35 transistor variations with approximately 8 each, were evaluated. For each unit a measurement of $1 / \beta$ at 7 emitter currents at each of 7 dose levels, resulted in approximately 12,600 data points. These figures are presented to illustrate the need for the use of the Hughes Automatic Data Acquisition System which has been described in a previous report (ref. 3). During the present program,measurements have been made of the base current rather than collector current which results in a direct determination of the parameter $1 / (\beta + 1)$ as opposed to common base current

gain α. The measurement circuit is essentially as shown in Figure 10. The value of R_B corresponding to a given emitter current was selected such that $I_E R_B = 10$. This being the case the voltage on the base resistor is given by

$$V_B = I_B R_B = \left[(I_E - I_B) / \beta \right] R_B = (I_E R_B - V_B) / \beta \tag{64}$$

thus

$$V_B = 10 / (1 + \beta) \quad . \tag{65}$$

The experimental values of V_B were processed by a computer. Data blocks which facilitated the plotting of $(1 / \beta)$ vs flux , β vs I_E , and β / β_o vs flux were printed out. Additionally, a least squares fit to the slope of $1 / \beta$ vs flux was obtained to characterize the radiation sensitivity. In addition to the value of reciprocal gain a measurement of leakage current, I'_{CBO} , above a threshold of 10 nA was made to correct DC β when necessary. For the mesa-planar comparison experiment the values of BV_{CBO} was monitored as well, since the primary effect is a modification of the base collector junction region.

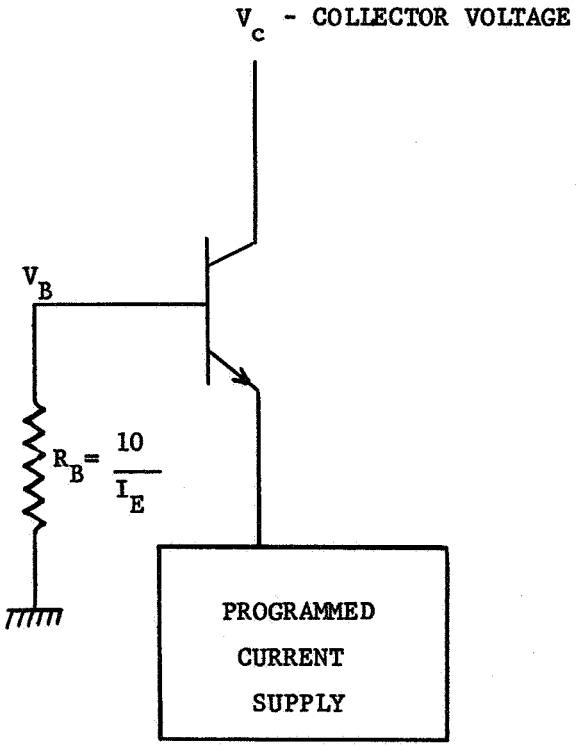

FIGURE 10 - ESSENTIALS OF MEASUREMENT CIRCUIT

Statistics

Basic to the statistical significance of each conclusion is the number of replications (six to eight in most cases) and the logical consistancy with expected results. Uncertainties due to process control were minimized by careful technique and a complete analysis of each transistor profile. Any unit which did not fit trends established by other variations was subjected to individual cross sectioning and review of process technique to establish reasons for variation.

The units for the emitter-to-base doping ratio variations and the four factor doping variations were organized as full factorial experiments (ref. 9). In the first case, referred to as emitter efficiency variations, the group consisted of ten each of nine variations in emitter and base profile combinations. The variations were accomplished by three levels of emitter diffusion into each of three levels of base diffusion for a single value of starting collector material.

In the second case, referred to as the factorial experiment, the four variables of junction depth, collector material, base doping and gold doping were produced at two levels of each factor in all combinations of factors for a total of sixteen variations.

Such an arrangement of factors lends itself to analysis by the technique of analysis of variance. The details of analysis of variance for the two factor level experiment receives an excellent discussion by Volk (ref. 10) and is not presented here. The end result is the assignment of a numerical confidence level to the significance

of each factor. The object of the analysis is a number for each variation representing a particular quantity such as radiation sensitivity, initial gain, breakdown voltage or other parameter.

Inability to maintain a tight control of parameters not being varied makes interpretation of interactions between design variables difficult and a complete knowledge of the profile will,in general, permit conclusions to be drawn without recourse to extensive statistical evaluation.

An additional statistical rule known as confounding (ref. 11) has been employed to determine the transistor grouping during irradiation. In general, the entire group of a factorial design is not irradiated as a unit. The technique of confounding is designed to eliminate any influence of dose variation between subgroups upon the estimation of variance due to main factors. Thus, when the factorial experiment was conducted at USC by irradiation in groups of four, the random variations in total dose was eliminated in computing the significance of design variations.

Device Irradiations

The majority of device irradiations were accomplished with 10 MeV electrons at the Hughes Research Linac. These electron irradiations were accomplished in a series of four tests over a period of six months. To confirm the conclusions drawn from these tests a sample of the devices were irradiated at the 30 MeV proton LINAC at the University of Southern California. A detailed comparison of the results from electron and proton irradiations is presented in a later section; at this point we will discuss the details of experimental procedure.

Electron irradiations. - The total fluence of 10 MeV electrons was accumulated by exposing the transistors to a series of three-microsecond pulses of 5×10^{11} electrons/cm^2. The electron fluence was determined by stopping the entire beam in a Faraday cup current monitor. The transistors were positioned four inches from the exit window where the beam has spread to approximately a 3/4" half-width. The distribution of beam intensity was determined by exposing a small diode detector at intervals across the beam, with the photocurrent serving as a measure of the relative beam intensity. From this data the number of electrons/cm^2 at the center was determined. The reproducibility of the pulse was frequently monitored by stopping part of the beam in a 5/8" diameter, 3/16" thick tungsten target.

The individual transistors were mounted in groups of 8 to 12, depending upon the optimum size of subgroup from the total (Statistics section), in a set of prepositioned sockets which permit selection from the control room. The transistor jig is shown in Figure 11. The transistors were unbiased with leads open during irradiation. At approximately seven fluence levels, I_{CBO} and β vs emitter current were measured.

Proton irradiations. - To provide confirmation of conclusions regarding design effects upon radiation resistance, the devices from the factorial experiment were irradiated at the University of Southern California Proton LINAC facility. In all, four each of the sixteen design variations were irradiated to a total fluence of 2×10^{13} protons/cm^2. The beam is pulsed at 280 pulses per second with an average beam current of 2 nA. The beam was passed through an ionization chamber which stopped approximately 4% of the beam. The exit from the ionization chamber was defined by a 1/2 inch collimator which would hold

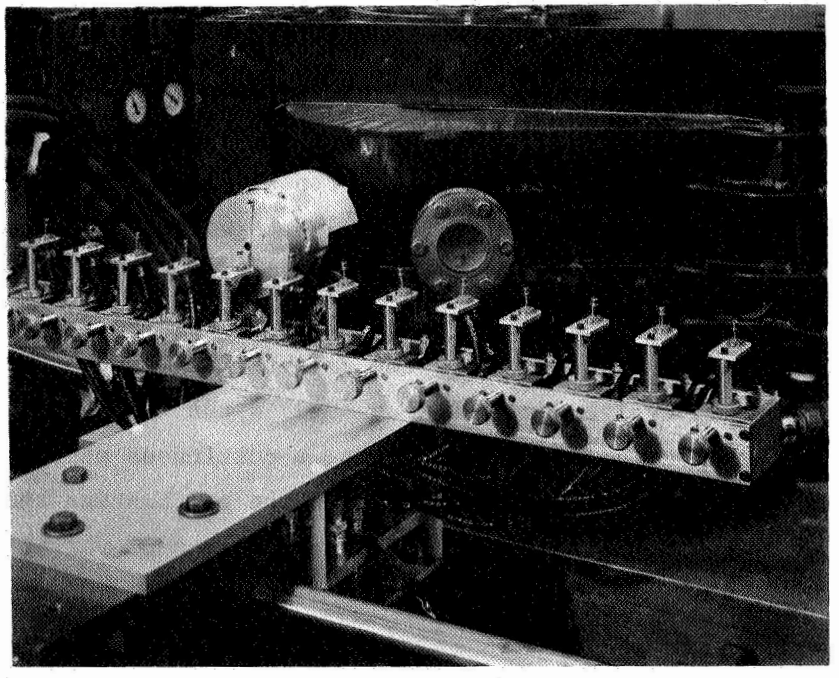

FIGURE 11 - AUTOMATIC TRANSISTOR POSITIONER
USED FOR ELECTRON IRRADIATIONS

four TO18 transistor cans. The transistors were mounted in a motor-driven socket to average asymmetries in beam density. This was, however, found to be unnecessary as glass slide exposures indicated the beam to be quite uniform.

The beam current was monitored by installation of an evacuated Faraday cup at the exit window. A schematic for the monitoring arrangement is shown in Figure 12. The beam current from the Faraday cup is passed into a $0.1\ \mu F$ capacitor connected to a high impedance electrometer circuit. Glass slide exposures had shown the beam distribution to be uniform and so the total fluence in a given period is just the capacitance times voltage divided by the area. While the total charge was being measured, the current from the ionization chamber was charging a $1\ \mu F$ capacitor. This voltage was fed into a circuit which put out a repetitive 9 volt ramp, discharging the capacitor each cycle to remain on a linear charging curve. This ramp was recorded on a chart recorder. The calibration was thus obtained in number of ramp cycles per unit fluence. As the ionization chamber remains in place during all irradiations, a continuous measure of the fluence was available. Several repeats of the calibration test during the course of the 18-hour run indicated less than a 3% variation in current density.

During irradiation, the transistors were unbiased with leads open. At approximately seven fluence levels, the transistors were subjected to a measurement of I_{CBO} and β as a function of emitter current.

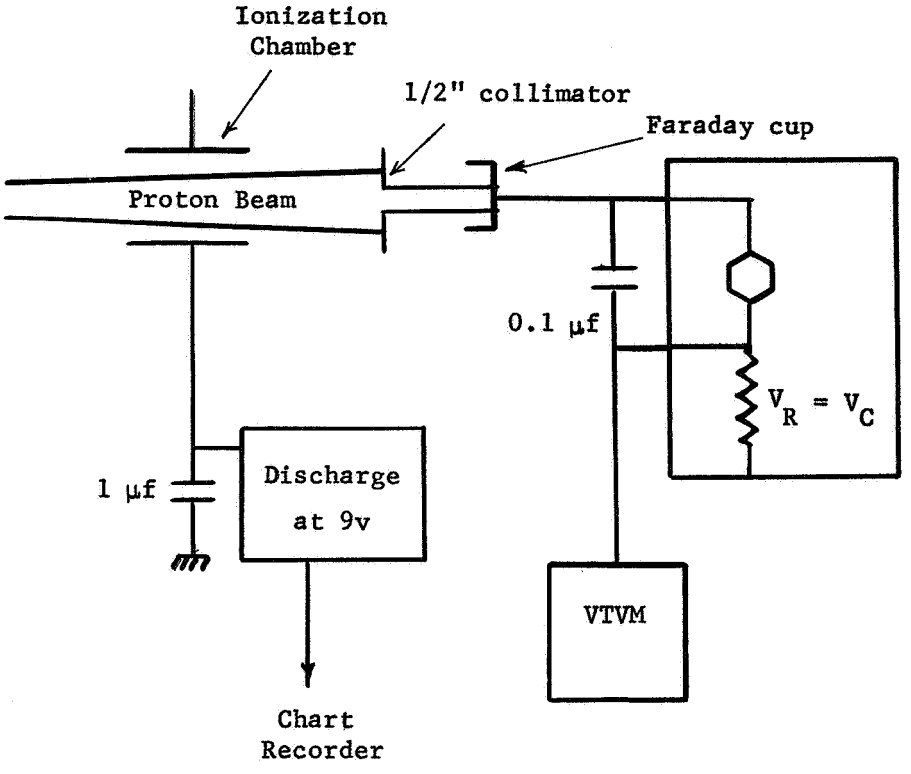

FIGURE 12 - PROTON BEAM
DOSIMETRY

EXPERIMENTAL DATA AND COMPARISON WITH THEORY

The experimental data and discussion in terms of profile parameters are presented here in the order in which the experiments were accomplished. These divisions are: (1) Comparison of mesa and planar processing, with and without passivation oxide; (2) Variations in emitter to base doping concentration (emitter efficiency); (3) Double diffused base structure; (4) 2^4 factorial designed experiment (doping profile variations); and, (5) Prototype units.

In a presentation of the data, two important features, both observed in a previous program (ref. 3), are to be noted: the linear dependence of reciprocal gain upon fluence and the dependence of $d (1/\beta) / d \phi$ upon emitter current. The general presentation of radiation damage data is in the form of $1/\beta$ as a function of fluence with emitter current as a parameter. Additionally, a cross plot of the data in the form of β vs emitter current with fluence as a parameter is shown for ease of device evaluation in a number of cases. Explicitly, profile parameters are recorded to permit analysis of transistor radiation sensitivity.

Comparison Of Mesa And Planar Processed Transistor Types

Previous experiments have indicated an unexpected behavior in mesa transistors in that the initial rate of change of β with flux was small or in a number of cases even positive. In an effort to evaluate this behavior mesa and planar transistors were fabricated with similar mask sets. During the period in which mesa processing was extensively employed in the semiconductor device industry, surface passivation was

not in general use. To include this lack of surface passivation as a factor, both mesa and planar units were produced with and without the surface oxide.

All units were produced on identical starting material, 5 Ω-cm epitaxial silicon on a low-resistivity substrate. The mesa units were formed by diffusing the base dopant over the entire wafer, forming the individual emitters and then defining the collector base junction by etching into the epitaxial material around an area defined by the base diffusion mask employed in the planar processing. These units were then completely stripped of oxide to obtain the mesa without oxide variation and to clean up the exposed junction. Half the mesa devices were then placed in a 985°C furnace with steam to grow approximately 2000Å of oxide.

As the primary differences between the mesa and planar units are of a geometrical character and surface treatment near the outer edge of the collector-base junction, a measurement of I_{CBO} and BV_{CBO} was performed at each fluence level.

Gain degradation data was taken on these units before the use of the automatic data system was available. For these units the common emitter current gain was measured by making a x-y plot of a voltage drop proportional to emitter current as a function of the voltage drop in the base resistor. The emitter current sweep was obtained by applying a voltage ramp to the emitter resistor which sets the current range.

The necessity to correct for leakage, I_{CBO}, may be seen from the expressions for total collector current,

$$I_C = I_E - I_B$$

$$I_C = \alpha I_E + I_{CBO} \qquad (66)$$

By eliminating I_C ,

$$(1 - \alpha) = (I_B + I_{CBO}) \ .$$

The reciprocal gain is given, in terms of common base current gain, by

$$1 / \beta = (1 - \alpha) / \alpha$$

thus,

$$1 / \beta = (I_B + I_{CBO}) / (I_C - I_{CBO})$$

Failure to correct for a significant leakage current would result in an overestimate of gain and possibly an increasing β with fluence when I_{CBO} is increasing.

The results of such corrected data are shown in Figures 13A and 13B for the planar configuration with and without oxide and in Figures 14A and 14B for the mesa variations. At currents above 5 mA, all devices exhibit approximately the same sensitivity to radiation as seen by the

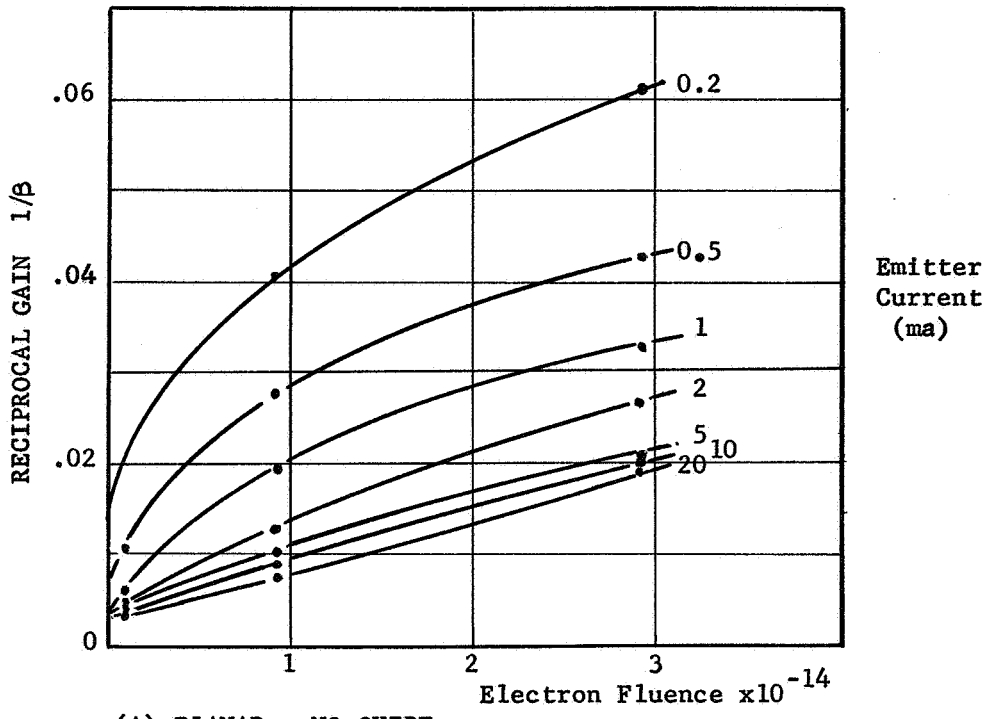

(A) PLANAR - NO OXIDE

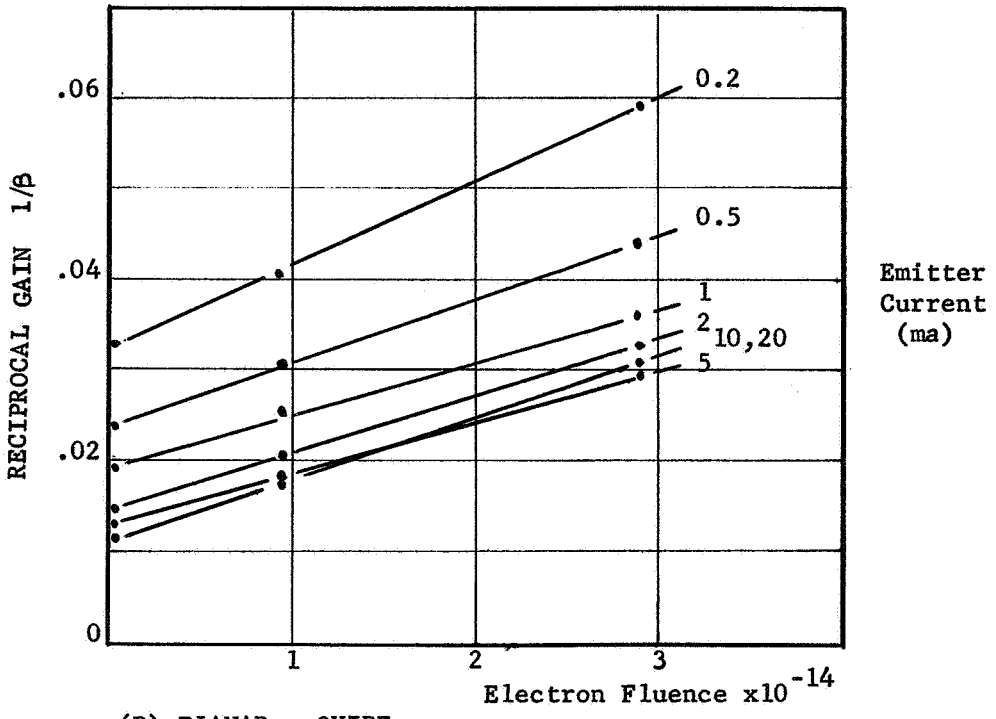

(B) PLANAR - OXIDE

FIGURE 13 - RADIATION INDUCED CHANGES IN COMMON BASE CURRENT GAIN

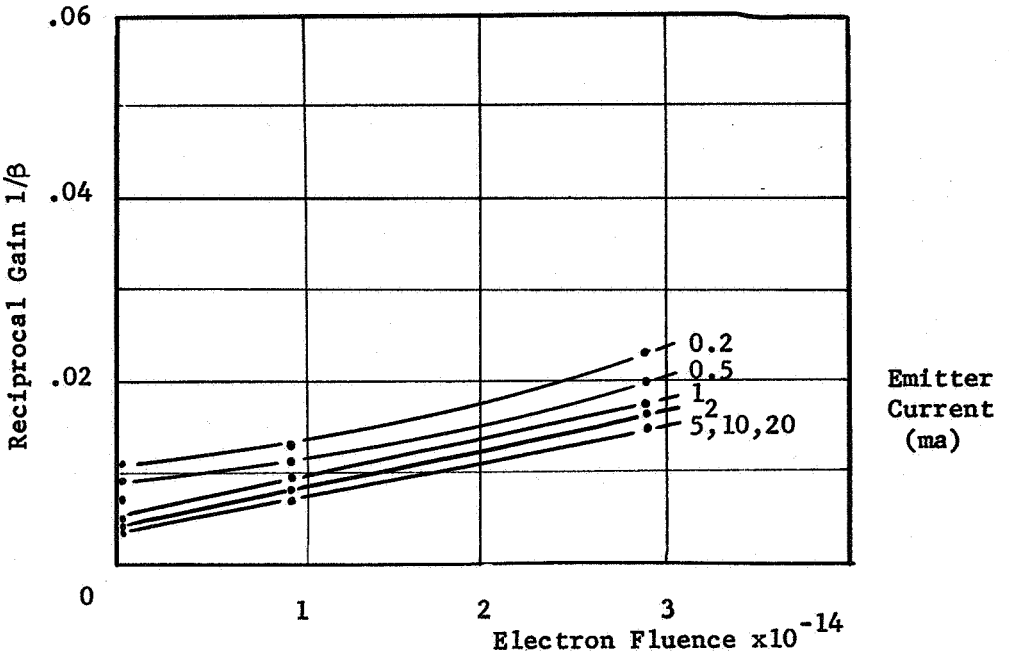

(A) Mesa - No Oxide

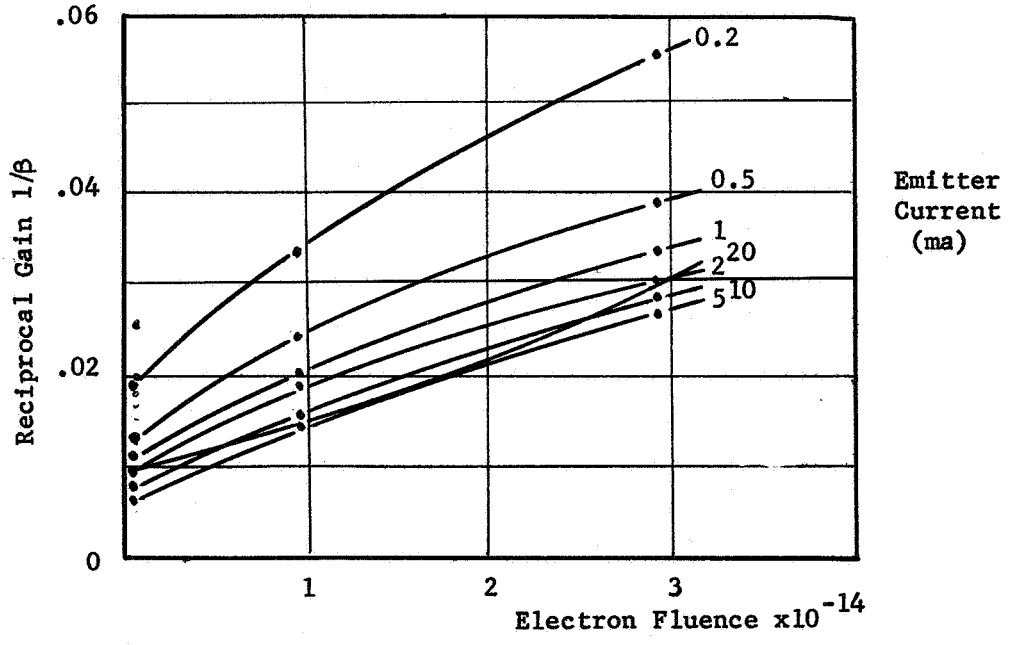

(B) Mesa - Oxide

FIGURE 14 - RADIATION INDUCED CHANGES
IN COMMON BASE CURRENT GAIN

slope of $1/\beta$ vs electron fluence. At lower currents the mesa without oxide appears more resistant but for this variation the leakage was most significant making an accurate measurement of $1/\beta$ difficult. The similarity of these curves demonstrates the bulk nature of the radiation effect as the differences between units is primarily surface configuration and treatment.

The behavior of reverse saturation current, I_{CBO}, differed greatly in these units. The planar no-oxide variation demonstrated such unstability as to make reproducible measurements difficult although a rapid increase to tens of microamps followed by a decrease to tens of nanoamps was evident. A similar result was noted for the mesa no-oxide variation which demonstrated large stable leakage currents. A representative example is shown in Figure 15A. Both mesa and planar devices with oxide displayed a linear increase of I_{CBO} in the subnanoamp range. Figure 15B illustrates the typical behavior of a planar with oxide variation.

At the levels of electron fluence obtained in this experiment, the breakdown voltages displayed little change with radiation, increasing slightly for some units and decreasing for others. Effects observed are probably due to a combination of factors such as changing collector resistivity and surface effects due to ionization in the surface oxides.

Variation In Emitter To Base Doping Ratio

During this phase the controlled variables were the resistivities of the emitter and base diffusion drives. The nine variations were accomplished by three levels of emitter diffusion into each of three

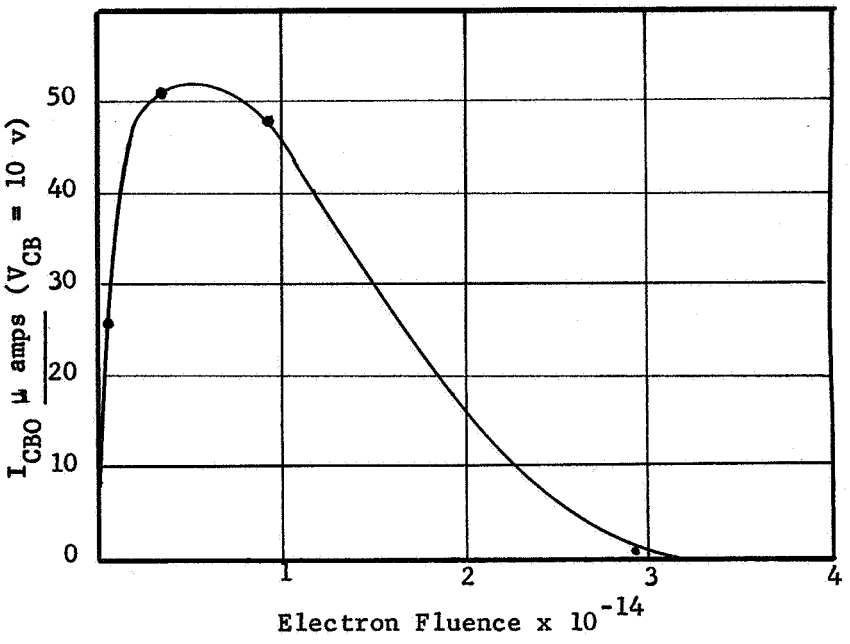

(A) Mesa - No Oxide

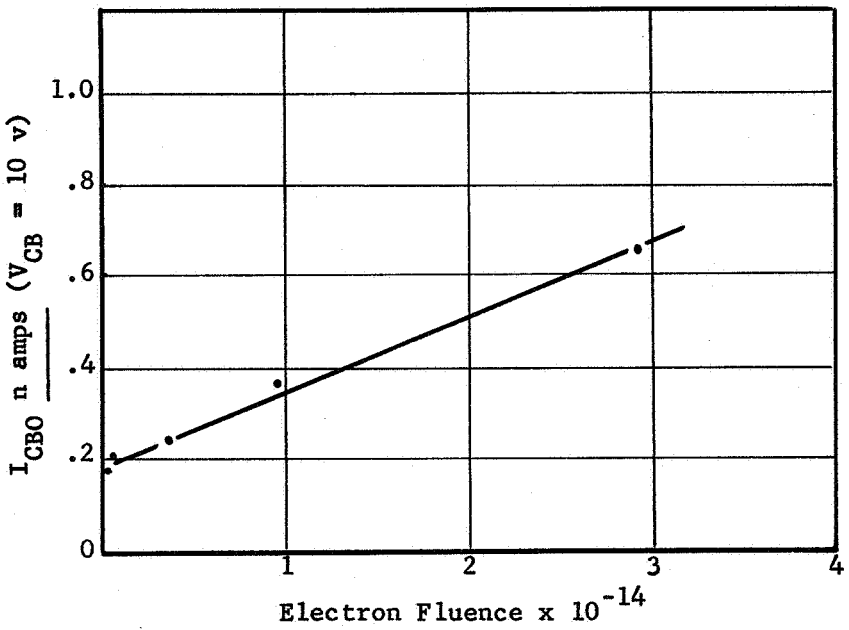

(B) Planar - With Oxide

FIGURE 15 - RADIATION INDUCED CHANGES IN I_{CBO}

levels of base diffusion. All units were produced on 2.5 Ω-cm collector material. In producing these units a number of unintentional variations in junction depth and base width occurred. The values of these resistivities and junction depths are given in Table 2 along with the base doping near the emitter edge of the base region.

TABLE 2-DESIGN PARAMETERS FOR EMITTER AND BASE DOPING RATIO VARIATIONS

Wafer Number	ρ_{sb} (Ω-cm)	ρ_{se} (Ω-cm)	x_{jb} (μ)	x_{je} (μ)	$N_A \times 10^{-16}$ (cm^{-3})
1	81	1.67	5.8	4.5	.58
2	81	1.81	5.8	3.8	1.99
3	81	2.72	4.6	2.6	4.44
4	135	1.67	5.6	3.7	1.55
5	135	1.81	5.2	2.9	3.27
6	135	2.72	5.2	3.5	1.40
7	215	1.67	5.5	3.7	1.12
8	215	1.81	5.2	3.2	1.71
9	215	2.72	5.5	3.6	1.24

Four each of these nine variations were irradiated to a fluence of 5×10^{14} electrons/cm^2. The results of these irradiations for the two experimental extremes of radiation sensitivity, groups 8 and 3, are shown in Figures 16 and 17. In Figure 16A and B, the data is presented as $1/\beta$ as a function of fluence with emitter current as a parameter. Figure 17 represents a cross plot of Figure 14 by displaying β as a

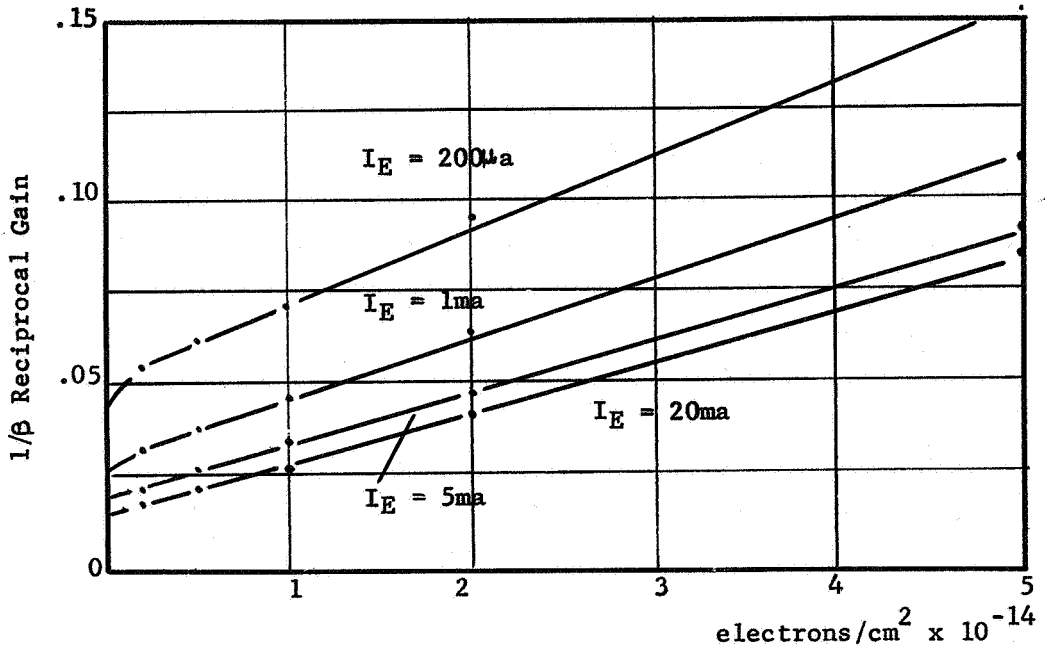

(A) Device No. 8

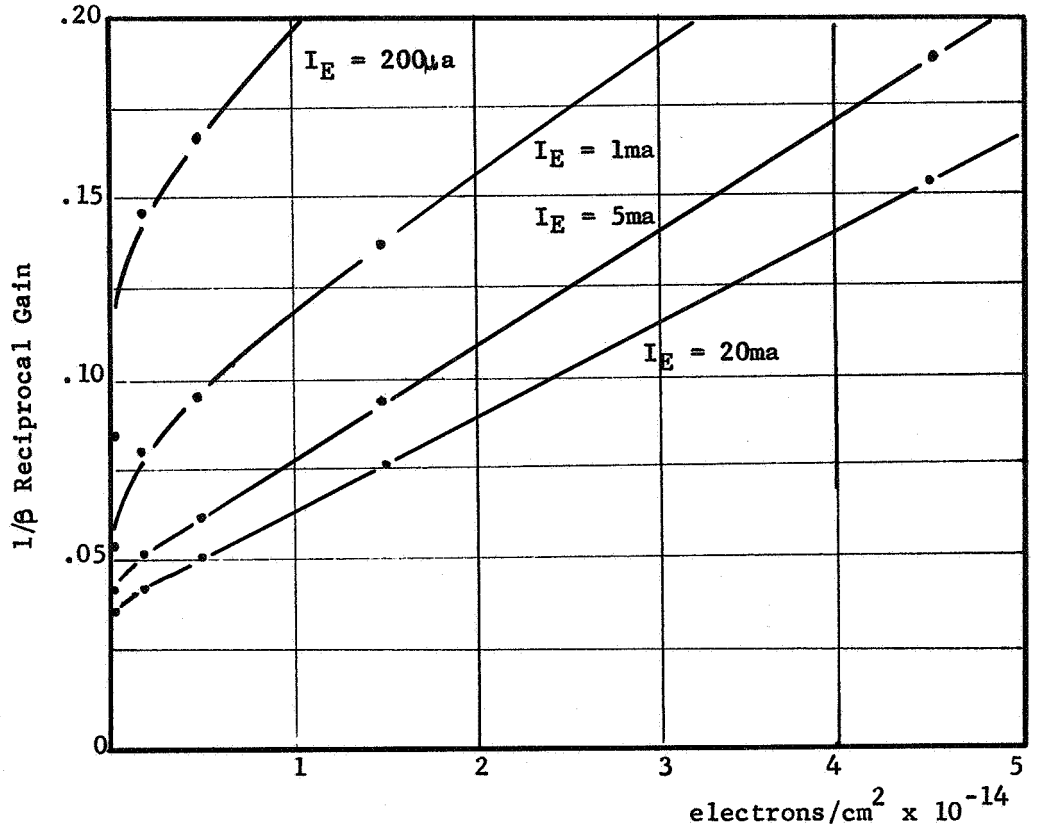

(B) Device No. 3

FIGURE 16 - RADIATION INDUCED CHANGES IN RECIPROCAL GAIN

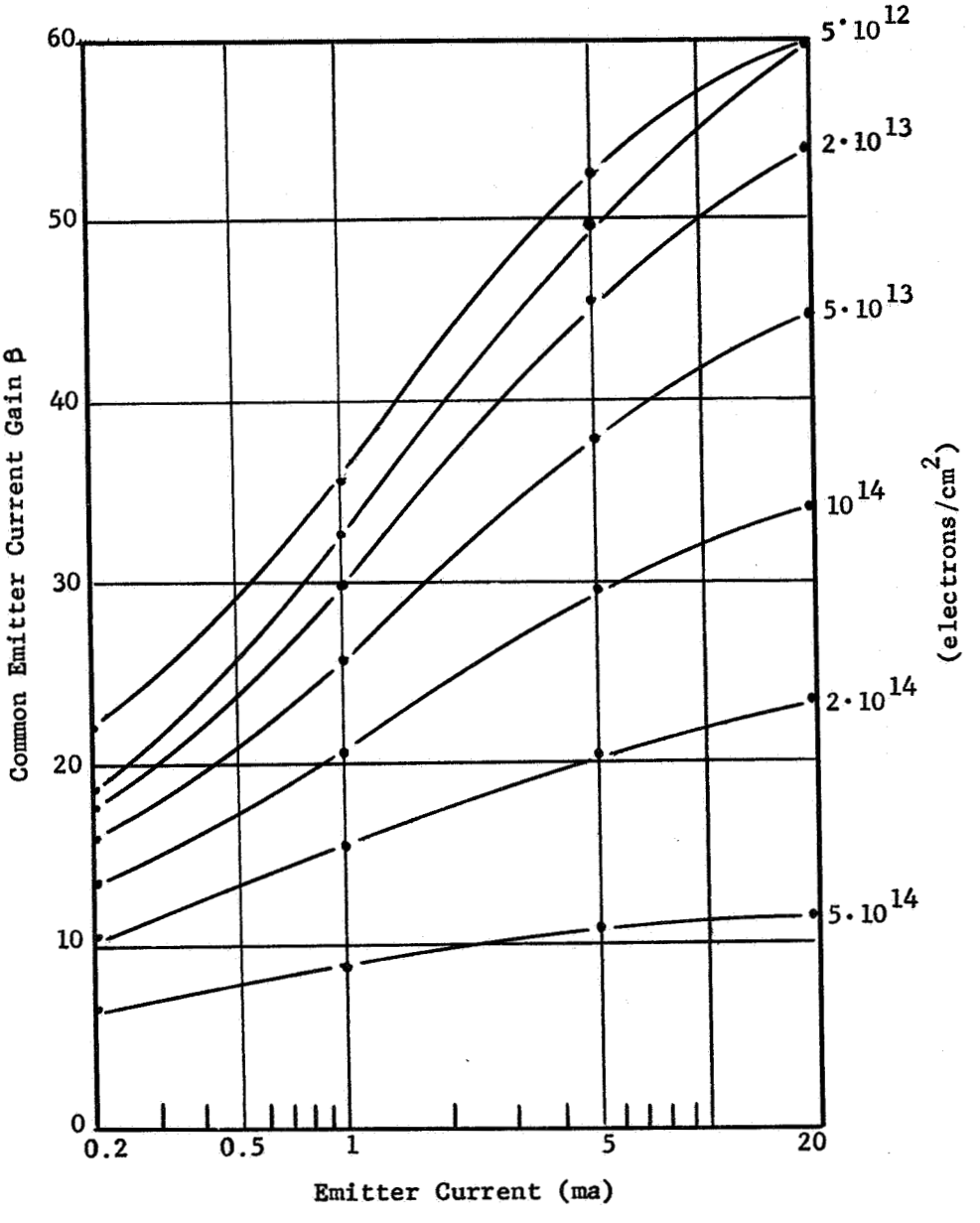

FIGURE 17A - GAIN CHARACTERISTIC
FOR IRRADIATED DEVICE NO. 8

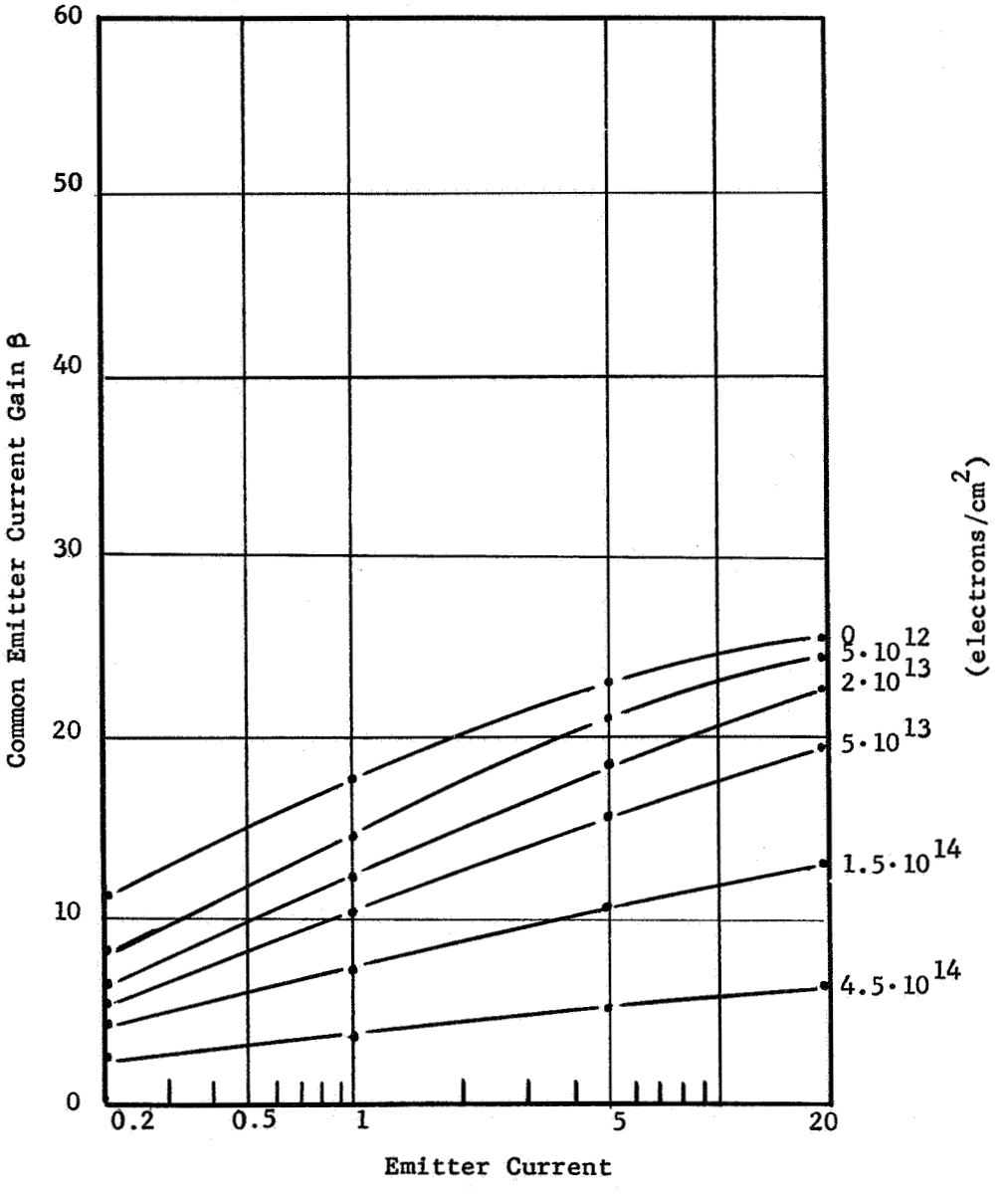

FIGURE 17B - GAIN CHARACTERISTIC
FOR IRRADIATED DEVICE NO. 3

function of emitter current with fluence as a parameter. A natural parameter to characterize the radiation sensitivity is the slope of the $1/\beta$ as a function of fluence curve. This slope is a function of emitter current (cf section on Composite Variation Of Radiation Sensitivity With Injection Level) and is shown in Figure 18 for groups 8 and 3 , and a group of intermediate sensitivity, group 4. The values of $d(1/\beta) / d\phi$ were calculated from an average of the slopes of a least squares fit to the data points above 10^{13} electrons/cm^2. These calculations for all nine variations are summarized in Table 3.

TABLE 3-RELATIVE RADIATION SENSITIVITY

Device Number	Relative Sensitivity*			
	200 μA	1 mA	5 mA	20 mA
8	1.90	1.64	1.38	1.32
7	1.86	1.70	1.50	1.40
1	2.52	2.03	1.76	1.71
2	2.76	2.16	1.78	1.56
4	2.98	2.16	1.76	1.51
9	3.00	2.26	1.84	1.66
6	3.36	2.63	2.16	1.84
5	3.98	3.37	2.72	2.25
3	5.00	3.74	3.11	2.55

* Numbers quoted are $d(1/\beta) / d\phi \times 10^{16}$ (electrons/cm^2)$^{-1}$

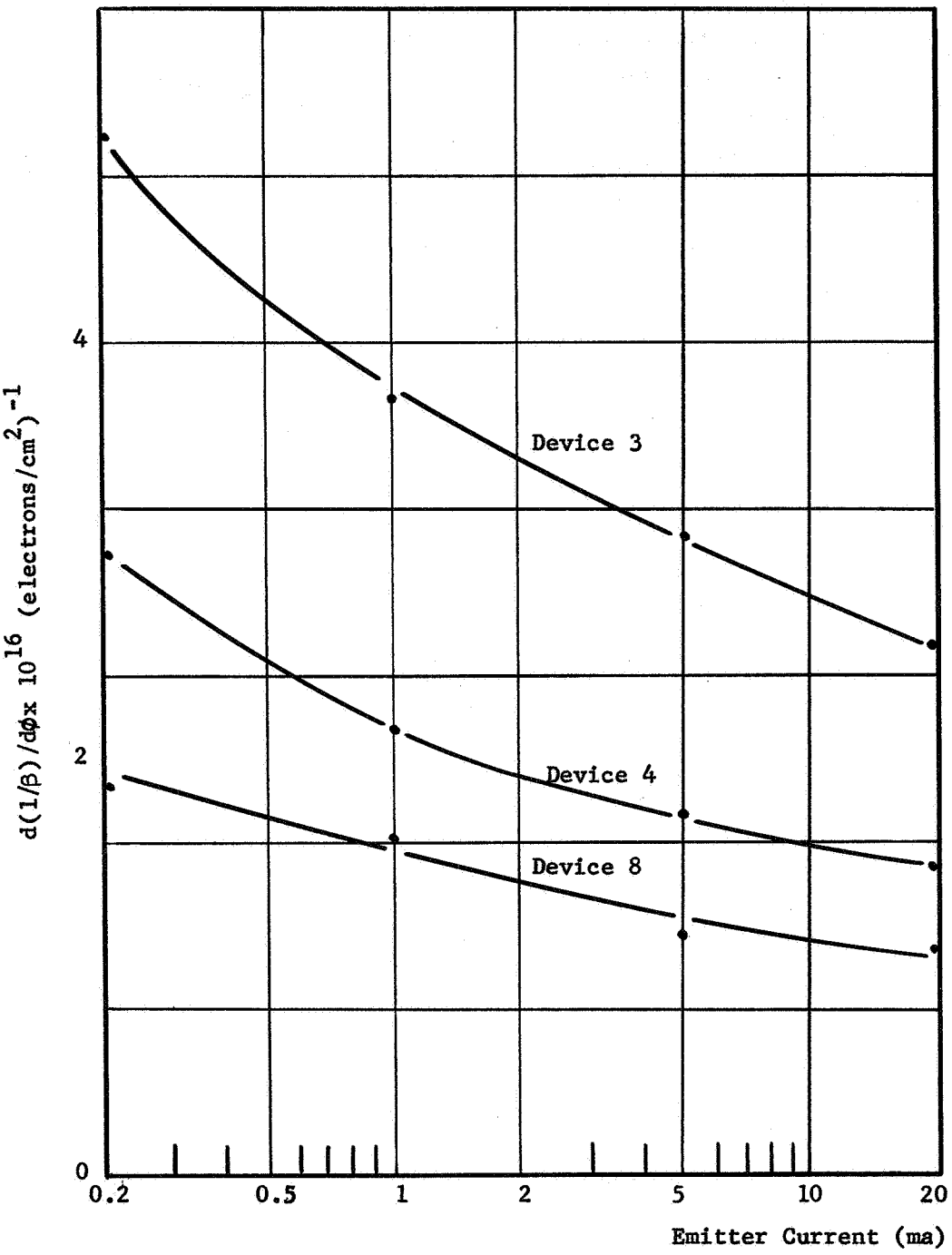

FIGURE 18 - INJECTION LEVEL EFFECTS ON DEGRADATION IN RECIPROCAL GAIN

The initial gain, β , was highest for groups 8 and 7 (36 - 41), lowest for groups 3 and 5 (13-16) and between these limits for all other units. Based upon the correlation with initial β , the data of Tables 2 and 3 and Figure 14, the following observations are made.

- As in the previous design variation program for the 2N708 the data appears highly linear after an initial rapid increase in $1/\beta$.

- An obvious injection level effect is present, as the injection level increases the radiation sensitivity decreases.

- The direction of the injection level effect supports the assumption of degradation in base transport with base lifetime as the controlling component. If the emitter efficiency were controlling the degradation, an increase of $d(1/\beta) / d\phi$ with current would occur; in accordance with the injection level effect for this component, contrary to observation.

- The linear data over the full range of emitter currents indicate there is no significant effect due to a decrease in effective emitter area in the injection level function. Thus, either the devices are in a state of high emitter crowding initially, or the highest base currents obtained do not produce significant crowding. The absence of a peak in the β vs I_E curves of Figures 17A and 17B support the latter argument.

- High base doping, which reduces base transport and emitter efficiency, correlates well with initial gain and radiation sensitivity.

If the base transport factor is controlling the slope of $1/\beta$ as a function of fluence, the variation in slope from low current to high current, as shown in Figure 18, should be proportional to the variation in $H(Z)$ for these units. The value of η is computed from an exponential approximation to the experimentally-determined profile. Using the data of Table 2 and an approximate diffusion constant (taken from Phillips, ref. 5, corresponding to the doping density of Table 2), the value of $Z = I_E W/(qDN_A A)$ is calculated for 200 μA and 20 mA. The value of $H(Z)$ may be determined from Figure 6. These calculations, including the ratio of $H(Z)$ at the two current levels are shown in Table 4 with the ratio of experimental slopes in the final column.

The agreement between theoretical and experimental values of relative sensitivity is considered excellent. A lower value for experimental sensitivity ratio would result from current crowding which decreases the effective emitter area.

TABLE 4-SUMMARY OF INJECTION LEVEL DATA

Device Number	η	Injection Level Parameter Z		Ratio of H(Z) Values H(20mA) / H(200 μA)	Ratio of Radiation Sensitivity *
		I_E=200 μA	I_E=20 mA		
1	3.0	0.0062	0.62	0.65	0.68
2	4.6	0.0027	0.27	0.71	0.57
3	5.9	0.0011	0.11	0.85	0.50
4	5.6	0.0030	0.30	0.68	0.50
5	5.5	0.0017	0.17	0.71	0.63
6	4.1	0.0033	0.33	0.68	0.55
7	4.0	0.0041	0.41	0.67	0.75
8	4.6	0.0028	0.28	0.71	0.70
9	4.0	0.0040	0.40	0.67	0.55

* From Table 3, Experimental Data

Double Diffused Base

The double diffused base structures include, in addition to the normal base diffusion, a second diffusion through a ring outside the emitter region. The doping profile of this ring diffusion is similar to the emitter profile, approximately 10^{20} cm^{-3} at the surface and equal in depth to the emitter, but of the same dopant as the normal base material. The effect of this diffusion is expected primarily in the edge injected base minority carriers. The basic configuration for the double diffused structures is shown in Figure 19. Minority carriers which are injected from the emitter edge will encounter a diffusion opposing field in the lateral direction and a strong aiding field in the direction of transport towards the collector. These fields are shown in Figure 20. Four designs were considered during this test. These include a standard transistor, no ring diffusion, two variations in the inner diameter of the enhanced ring and two variations in base profile of one ring diameter.

Subsequent to the device irradiations, angle cross sections of the large diameter unit indicated the base width was considerably less than that of the other units, thus limiting the validity of comparison between these units.

The irradiation data on these units is summarized in Figure 21 in a plot of $d(1/\beta) / d\phi$ as a function of emitter current. The

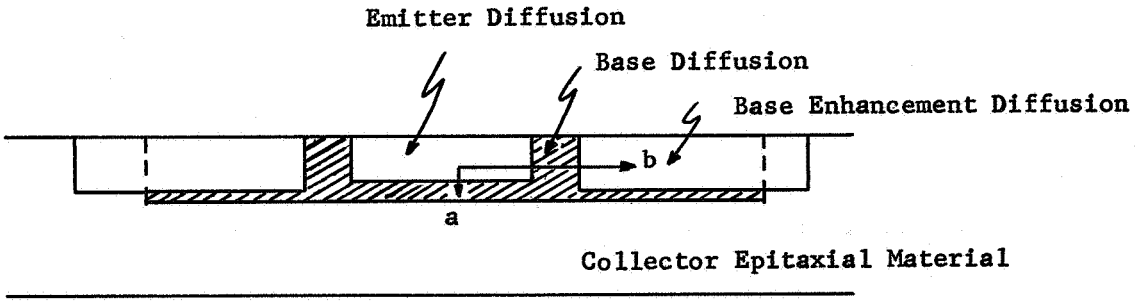

Figure 19 - Double Diffused Base Transistor

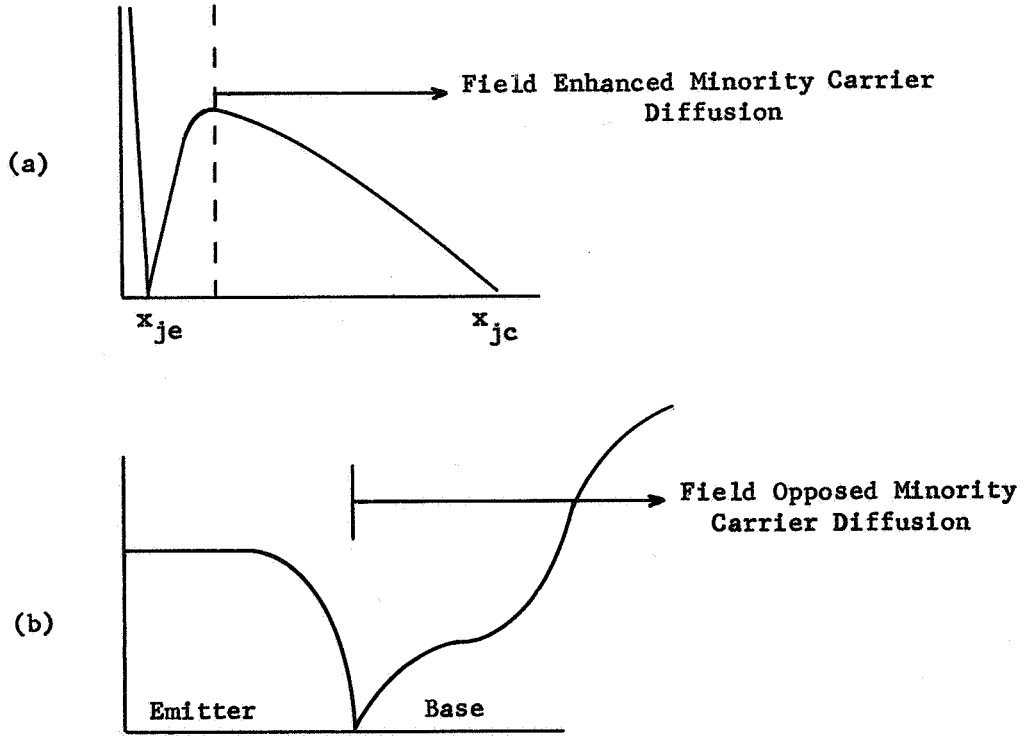

Figure 20 -Doping Profile and Effect Upon Minority Carrier Diffusion
a. Normal Injection Path into Base
b. Lateral Injection into Base

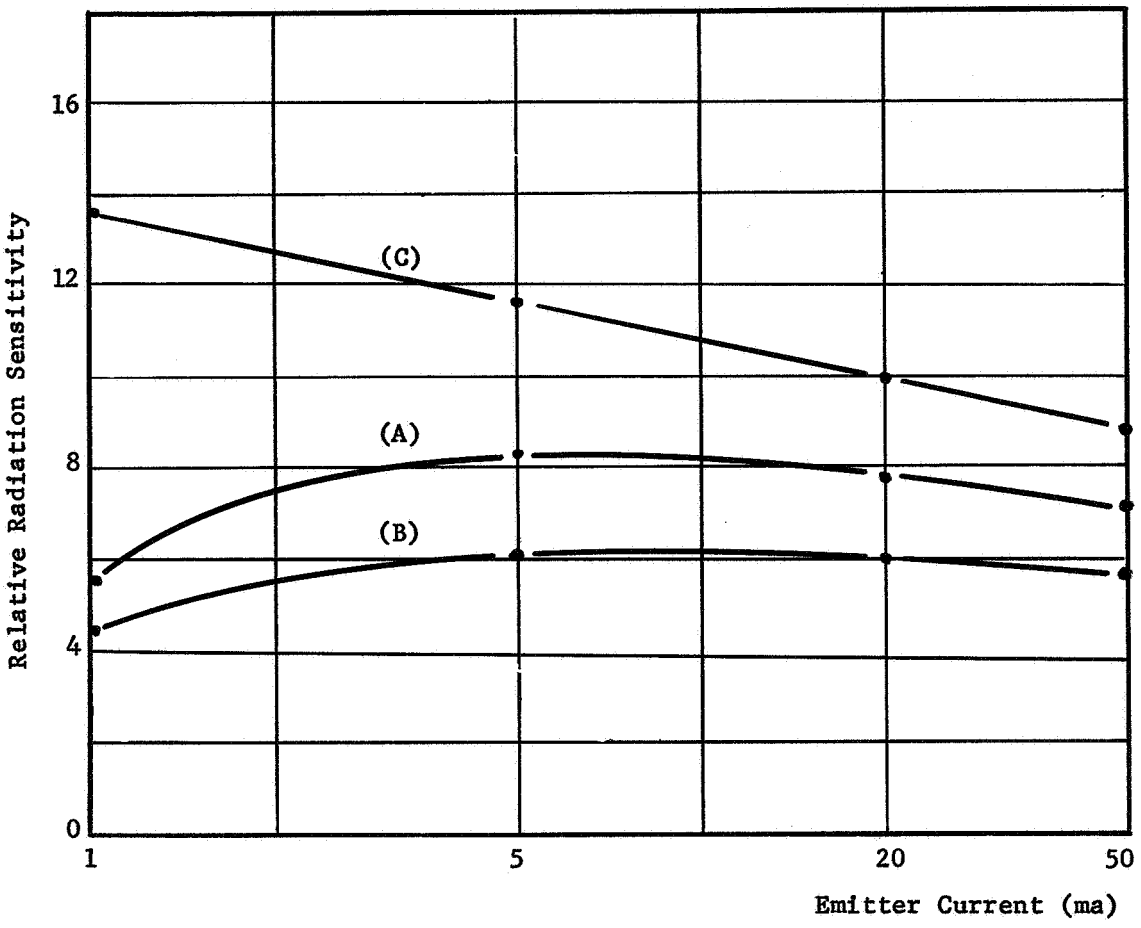

FIGURE 21 - RELATIVE RATE OF CHANGE OF $1/\beta$ FOR VARIATIONS OF DOUBLE DIFFUSED BASE TRANSISTORS

(A) STANDARD TRANSISTOR
(B) DOUBLE DIFFUSED BASE ($W = 1.7_{\mu}$)
(C) DOUBLE DIFFUSED BASE ($W = 2.5_{\mu}$)

standard device falls between the two double diffused structures in radiation sensitivity. No strong effects due to the double diffused structure are evident. The variation in radiation sensitivity is explained in part by the base width variation in these devices. Device A, the standard transistor has a 2.3 micron base width while devices C and D are 1.7 and 2.5 microns respectively.

Factorial Designed Experiment

A full factorial experimental arrangement consists of evaluating the effects of individual parameters (factors) at each value of all the additional factors (factor levels). The factors selected for evaluation are the collector resistivity, the doping junction depths, the base drive surface concentration, and the presence or absence of gold doping. Each factor was evaluated at two levels making a total of 16 design variations. The actual design parameters achieved are shown in Table 5. These values differ from the desired levels due to normal variations in production, the difficulty in obtaining the desired diffusion profile without excessive trial runs, and the errors involved in measurement of the profile parameters.

These 16 variations were evaluated under both electron and proton irradiation as discussed in the previous section on experimental procedure. The results of these irradiations indicate conclusions as to doping and doping profile effects on radiation sensitivity are the same for both electron and proton irradiations. A summary of the relative radiation sensitivity, as characterized by $d(1/\beta) / d\phi$, is given in Tables 6 and 7 for electron and proton irradiation respectively.

TABLE 5-DESIGN PARAMETERS FOR FACTORIAL EXPERIMENT

	Collector Resistivity Ω-cm	Collector Base Junction Depth x_{jb} Micron	Base Width W Micron	Base Drive Surface Concentration C_{ob} cm^{-3} ($\times 10^{-18}$)	Emitter Drive Surface Concentration C_{oe} cm^{-3} ($\times 10^{-20}$)	Gold
1	2.5	3.8	1.5	.80	6.4	No
2	2.5	4.1	1.5	.70	5.0	
3	2.5	4.6	1.7	8.00	3.8	No
4	2.5	5.1	1.5	7.20	3.0	
5	2.5	5.8	2.6	.78	4.3	No
6	2.5	5.8	1.7	1.00	5.2	
7	2.5	5.2	1.5	8.20	3.4	No
8	2.5	5.9	1.7	6.40	3.2	
9	.56	3.5	1.2	.76	6.4	No
10	.56	3.3	1.2	1.20	9.2	
11	.56	4.1	1.5	8.40	5.2	No
12	.56	5.0	1.0	7.40	2.6	
13	.56	5.2	2.0	.76	4.3	No
14	.56	5.2	1.9	.77	4.2	
15	.56	5.5	1.7	6.70	3.3	No
16	.56	5.5	1.3	7.20	3.1	

TABLE 6-ORDER OF DECREASING RADIATION SENSITIVITY OF SIXTEEN DESIGN VARIATIONS UNDER ELECTRON IRRADIATION

$\left[K = d\left(1/\beta\right) / d\phi \times 10^{16}\ (\text{electrons/cm}^2)^{-1}\right]$

I_E=200 μA		I_E = 5 mA		I_E = 50 mA	
Device Number	K_1	Device Number	K_2	Device Number	K_3
7	4.94	7	2.50	6	2.02
11	4.32	5	2.40	4	1.98
15	4.00	11	2.12	5	1.88
8	3.74	15	2.04	8	1.86
5	3.56	8	1.78	7	1.72
14	3.16	13	1.60	15	1.42
13	3.08	14	1.58	11	1.38
3	2.90	3	1.42	13	1.20
16	2.78	16	1.42	14	1.18
6	2.70	6	1.38	3	1.16
4	2.22	4	1.10	16	1.04
1	1.68	1	.80	1	.88
12	1.34	2	.76	2	.86
2	1.22	9	.72	9	.74
9	1.04	12	.62	12	.68
10	-	10	.50	10	.58

TABLE 7-ORDER OF DECREASING RADIATION SENSITIVITY OF SIXTEEN DESIGN VARIATIONS UNDER PROTON IRRADIATION

$\left[K = d\left(1/\beta\right)/d\phi \times 10^{15}\ (\text{protons/cm}^2)^{-1}\right]$

I_E=200 μa		I_E = 5 mA		I_E = 50 mA	
Device Number	K_1	Device Number	K_2	Device Number	K_3
7	19.34	7	8.16	6	5.87
15	17.32	15	7.75	7	5.10
11	15.40	14	6.61	4	4.97
14	14.87	11	6.52	15	4.72
5	14.41	5	6.42	14	4.34
16	12.17	6	5.25	11	3.95
13	11.79	13	5.07	5	3.95
8	10.75	16	4.83	8	3.64
6	10.61	8	4.60	16	3.60
3	8.40	3	3.77	13	3.00
4	7.95	4	3.45	3	2.58
1	6.61	1	2.89	1	1.88
12	5.61	10	2.48	2	1.94
9	5.45	12	2.43	9	1.57
10	5.32	9	2.41	12	1.54
2	4.95	2	2.30	10	1.51

The factors determining radiation sensitivity; i.e., base transport and emitter efficiency, depend strongly upon the base doping profile. The experimentally determined base doping profiles are presented in Figure 22 for six of the sixteen variations (groups 1, 2, 8, 11, 12 and 15).

From a comparison of the data in Tables 6 and 7 with the profiles in Figure 22, several points may be made. The variations 1, 2, 9 and 10 are,as a group, the variations with the most shallow junctions. Together with device 12 they are consistently superior in radiation resistance. Shallow junctions at fixed total doping concentrations imply both the base field parameter, η , and the linear grade constant, a , will be relatively higher. As seen in Equations 62 and 63 both effects are observed to decrease the slope of $1 / \beta$ vs flux.

Device 12, although not having shallow junctions, has a combination of low net doping and narrow base width. Again from Equations 62 and 63 these features are seen to reduce radiation sensitivity.

Device 11 has the highest doping density but moderately shallow junctions. Device 15 has a moderately high doping density and deep junctions and device 8, with a lighter doping density, has the deepest junctions of all the variations. Device 5 has the combination of high doping and wide base width. As expected from Equations 62 and 63, these units are all among the most radiation sensitive variations.

Device 6,which displays a low sensitivity at low currents and tops the list at high currents, has a lighter doping than device 12 but a significantly larger base width and junction depth.

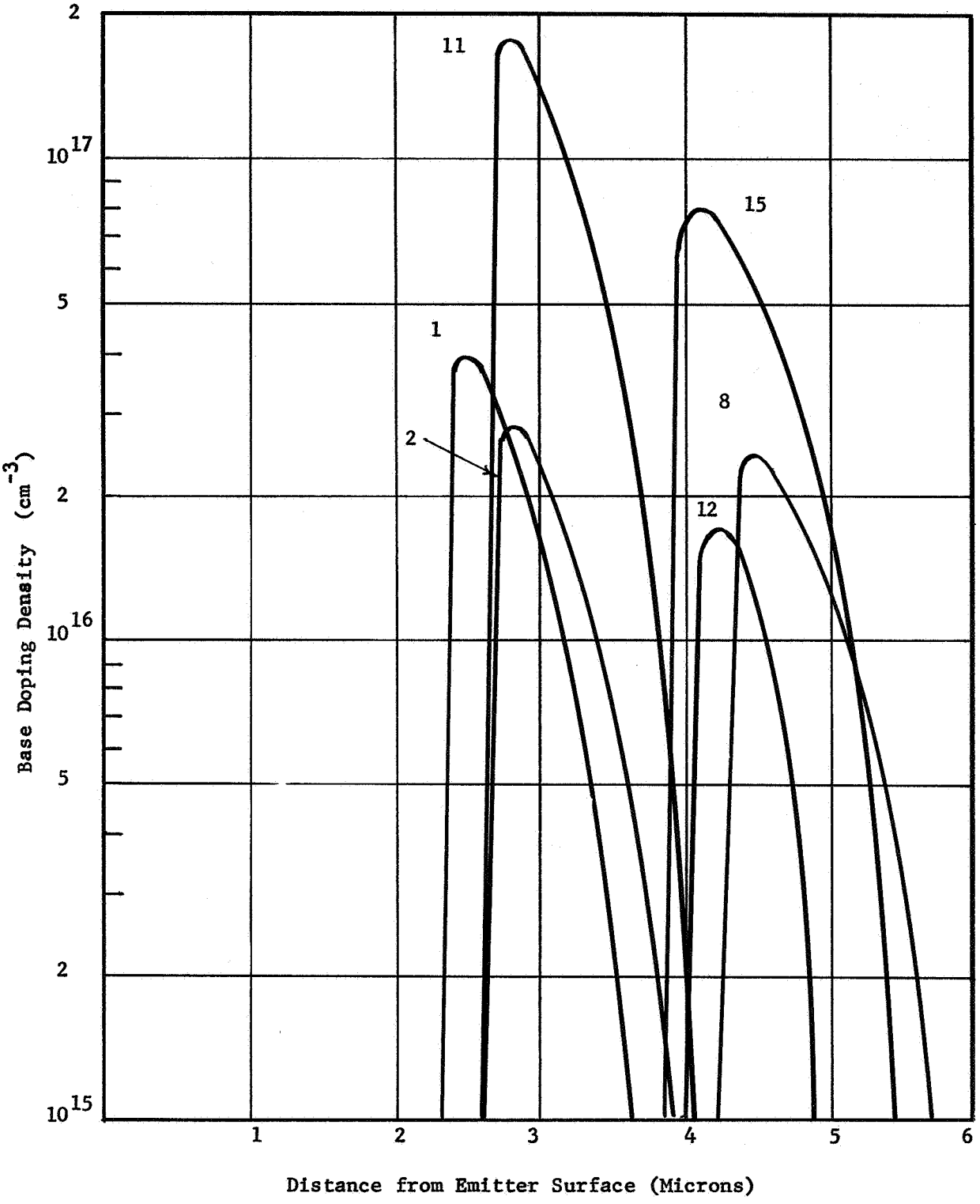

FIGURE 22 - BASE DOPING PROFILES FROM FACTORIAL EXPERIMENT

Devices 7 and 3 do not fit the above pattern of correlation between doping profile and radiation sensitivity, this may be due to errors in profile determination as the correlation is well established by the other units.

No significant correlation with junction breakdown voltages was established in these sixteen design variations. At 5 mA, the average gain of devices 1, 2, 9, 10 and 12 was 125, while the five most sensitive units (7, 5, 11, 15 and 8) had an average gain of 50.

Design Verification

To demonstrate the validity of the design criteria developed in the preceding sections, a final phase of transistor design and radiation testing was conducted. As the collector doping and gold concentration did not appear critical, they were taken at the low value (2 Ω-cm, no gold) to provide good breakdown and gain characteristics respectively. The base and emitter junction depths were shallower than those of the previous section and the base width decreased ($x_{jb} = 2\,\mu$, $x_{je} = 1.4\,\mu$, $W = 0.6\mu$). The peak base doping was held as low as the least of the sixteen design variations presented in the previous section. The complete profile is shown in Figure 23.

These devices were irradiated with the same sequence of electron dose increments as those variations described in the previous sections. A plot of $1/\beta$ vs fluence for $I_E = 5$ mA is shown in Figure 24 for the radiation resistant prototype along with the corresponding curve for design variations 9, 16 and 5 of the preceding section. A summary plot of $d(1/\beta) / d\,\phi$ vs emitter current is shown in Figure 25 for these four design variations. The data for each device represents the average response from irradiation data on six replications.

The preirradiation electrical test data for these same four groups is given in Table 8. The performance of the radiation resistant unit is comparable or superior in each regard.

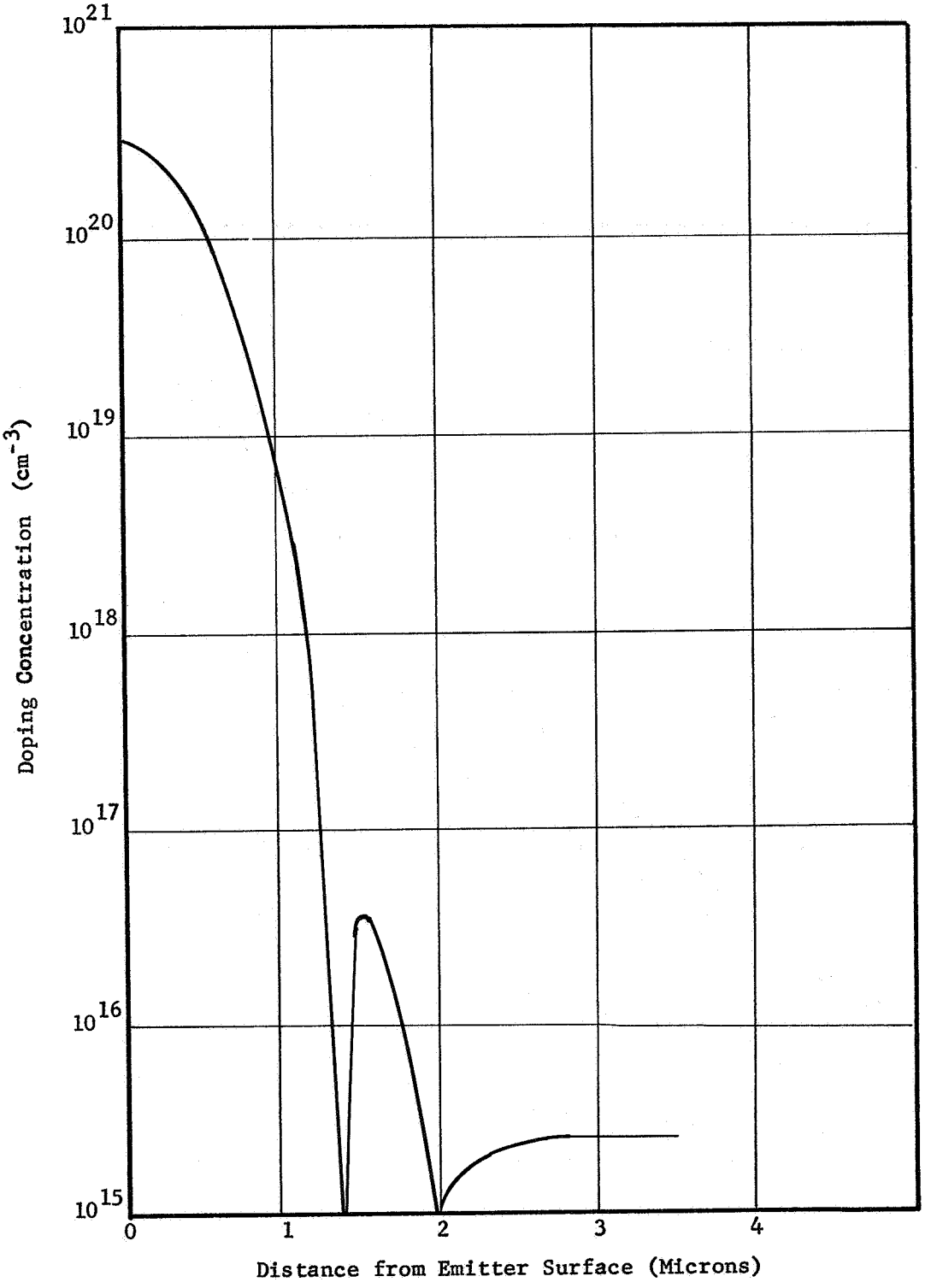

FIGURE 23 - TRANSISTOR DOPING PROFILE
FOR DESIGN VERIFICATION

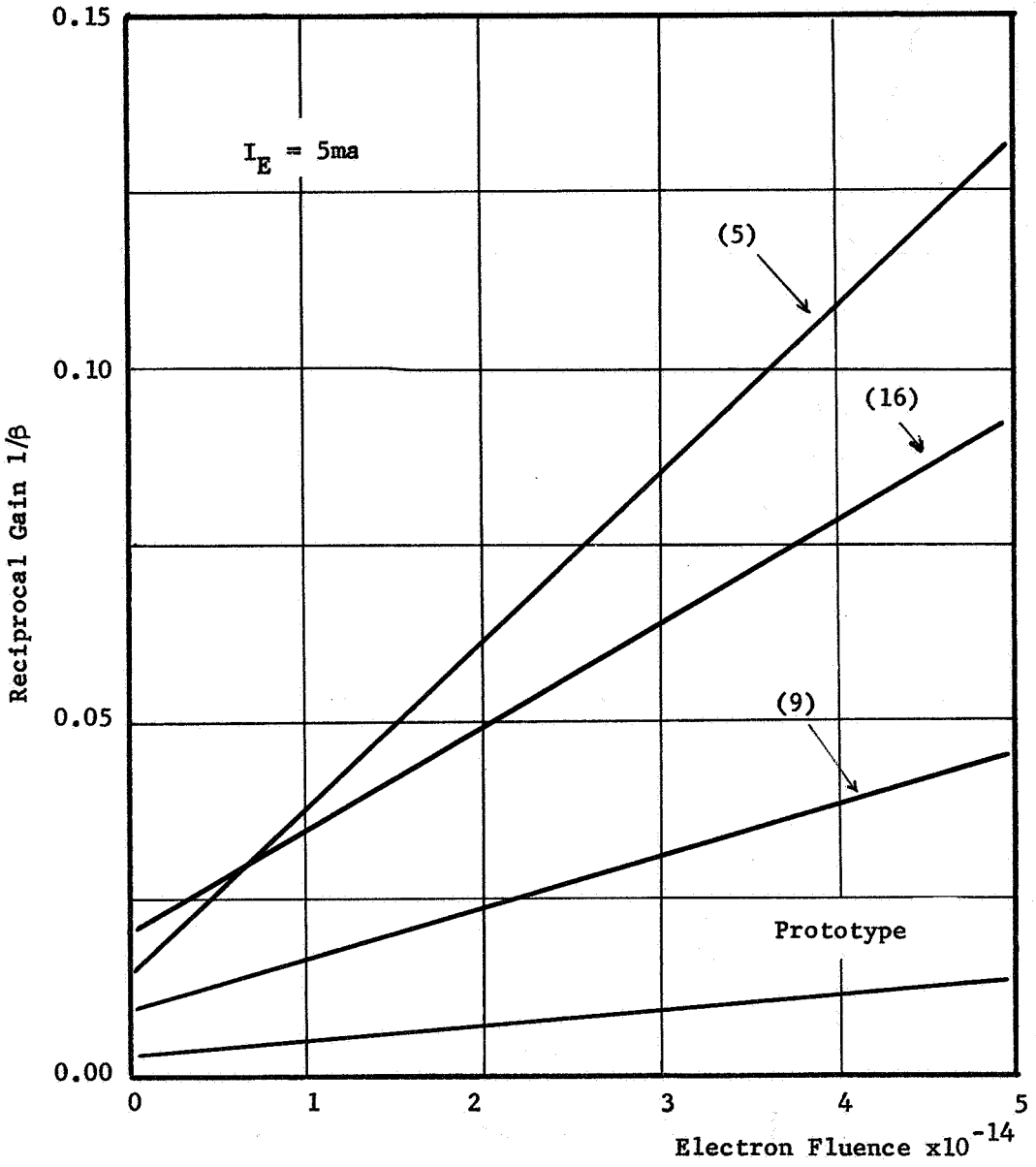

FIGURE 24 - RADIATION INDUCED CHANGES IN RECIPROCAL GAIN FOR GROUPS 5,16,9 AND THE RADIATION RESISTANT PROTOTYPE

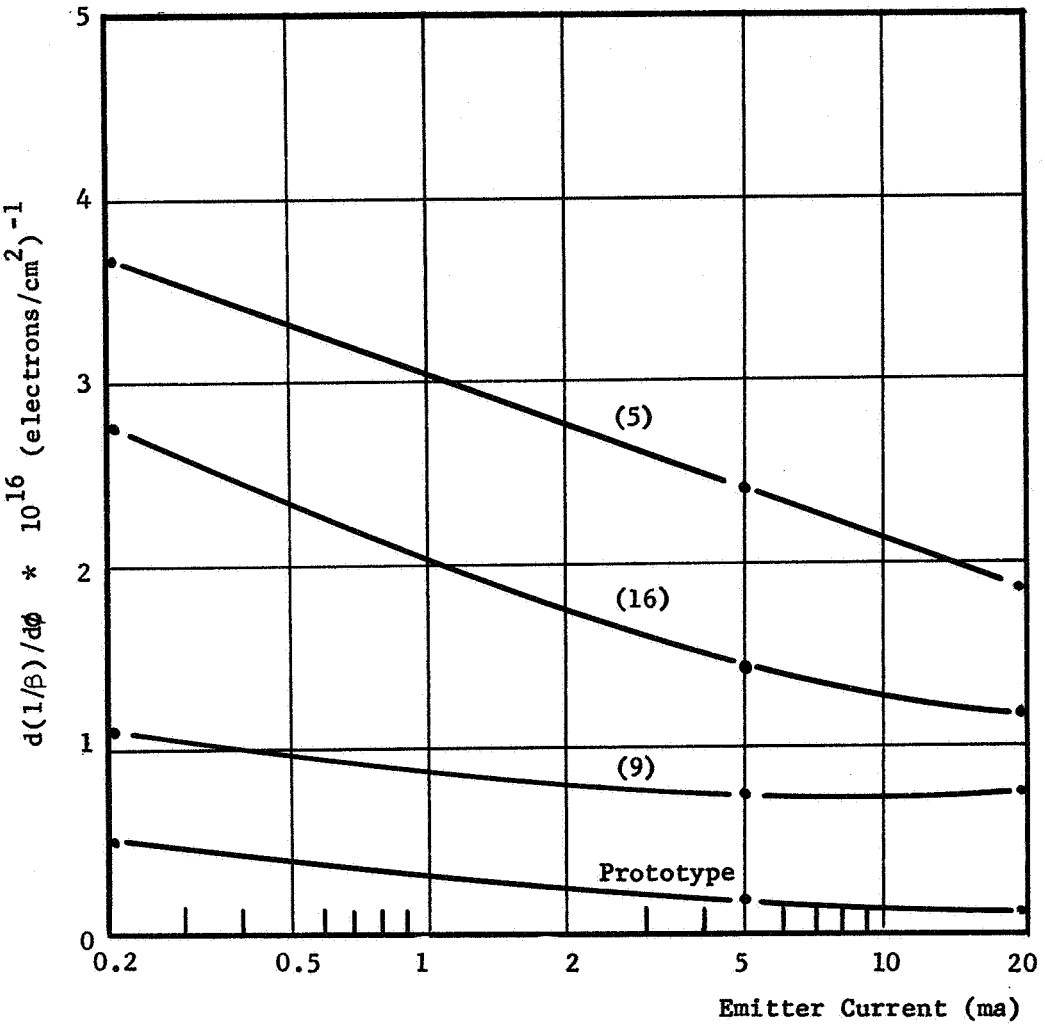

FIGURE 25 - COMPARISON OF PROTOTYPE AND SELECTED VARIATIONS FROM FACTORIAL EXPERIMENT. INJECTION LEVEL EFFECTS ON RECIPROCAL GAIN DEGRADATION

TABLE 8-PREIRRADIATION TEST DATA FOR RADIATION RESISTANT PROTOTYPE AND REPRESENTATIVE DEVICES FROM FACTORIAL EXPERIMENT

Device Number	β I_E=5 mA	BV_{CBO} Volts	BV_{CEO} Volts	BV_{EBO} Volts	$V_{CE\ SAT}$ Volts
Prototype	132	76	63	6.0	0.09
10	64	77	28	10.0	0.21
16	51	72	31	7.2	0.22
5	40	140	60	9.5	0.08

CONCLUSIONS

The principal conclusions, based upon analysis of experimental results and theoretical developments accomplished during the present design effects study, include:

- For a given value of base width, the junction depths should be as shallow as consistent with transistor specifications. These considerations will include breakdown voltages and low current gain. Improvements result from an increase in emitter and base doping gradient.

- Low base doping contributes to radiation resistance through base injection level effect and emitter efficiency.

- Gold doping appears to provide radiation resistance at current levels below the peak of β vs I_E. Association of gold doping with high $V_{CE\ SAT}$ and low β represent design trade-offs.

- Collector doping variations in the range of $2 \cdot 10^{15}$ to 10^{16} did not significantly affect radiation resistance.

- Mesa configuration does not offer any superiority over the planar in radiation sensitivity of common emitter current gain. Previous data in which the mesa had an apparently increasing β may have been due to an increase in I_{CBO}.

- Importance of a determination of base profile is demonstrated through an injection level analysis of β degradation with doping profile as a parameter.

CONCLUSIONS (continued)

- Explicit dependence of emitter efficiency upon design variables is shown to predict a linear degradation with radiation fluence.

APPENDIX 1

Minority Carrier Distribution In Emitter Region

Equation 44, subject to boundry conditions of Equation 45, yields the two algebraic equations

$$p(0) = A + B \tag{A1}$$

$$0 = A \exp (m_1 \ell) + B \exp (m_2 \ell) \tag{A2}$$

where $\ell = x_{je} - x_{eb}$

Solving for A and B

$$A = p(0) \exp (m_2 \ell) \; / \; \left[\exp (m_2 \ell) - \exp (m_1 \ell) \right] \tag{A3}$$

$$B = p(0) \exp (m_1 \ell) \; / \; \left[\exp (m_1 \ell) - \exp (m_2 \ell) \right] \tag{A4}$$

With these coefficients Equation 43 is given as,

$$p(x) = \frac{p(0)}{\exp (m_1 \ell) - \exp (m_2 \ell)} \left[\exp (m_1 \ell + m_2 x) - \exp (m_2 \ell + m_1 x) \right] \tag{A5}$$

We may factor out and cancel a common factor of $\exp (- \ell / 2 x_e)$. Substitute

$$\alpha = \left[1 + 4 (x_e / L_{pe})^2 \right]^{\frac{1}{2}} \Big/ 2 x_e = (m_1 + m_2) / 2 \qquad \text{(A6)}$$

into Equation A5 to obtain,

$$p(x) = \frac{p(0) \exp (- x / 2 x_e)}{\sinh (\alpha x_e)} \sinh \left[\alpha (\ell - x) \right] . \qquad \text{(A7)}$$

Expand

$$\sinh (\alpha \ell - \alpha x) = \sinh (\alpha \ell) \cosh (\alpha x) - \cosh (\alpha \ell) \sinh \alpha x . \qquad \text{(A8)}$$

For a typical emitter profile we will have $x_e < L_{pe}$ and $\ell \gg x_e$, thus $\sinh (\alpha \ell) \approx \cosh \alpha \ell$. Using this approximation, Equation A5 becomes

$$
\begin{aligned}
p(x) &= p(0)\ \exp\left(-x / 2x_e\right)\ \left[\cosh\left(\alpha x\right) - \sinh \alpha x\right] \\
&= p(0)\ \exp\left(-x / 2x_e\right)\ \left[\exp\left(-\alpha x\right)\right] \qquad \text{(A9)} \\
&= p(0)\ \exp\left\{-\left[1 + \left(1 + 4\left(x_e/L_{pe}\right)^2\right)^{\frac{1}{2}}\right]\left(x / 2x_e\right)\right\}
\end{aligned}
$$

APPENDIX 2

Proton Irradiation of Insulated Gate Tetrode

The present contract, in addition to the bipolar study, called for a limited amount of effort with a contemporary majority carrier device. The device chosen for investigation was a newly developed insulated gate tetrode.

In its usual configuration, the insulated gate field effect transistor consists of a metal gate that overlaps both source and drain electrodes. This is necessary in order to fully modulate the channel region. There are two disadvantages, however, with this configuration. First, the maximum operating drain voltage is limited, for an n-channel device, for example, to about 40 volts. Second, the gate overlap results in a high gate-to-drain capacity that affects the input capacity of the device; an effect similar to the Miller effect in the vacuum tube.

The insulated gate tetrode, (IGT), employing a second gate and insulator stacked over the first gate with its insulator, has been developed to overcome these limitations. It is illustrated in Figure A1. Because of the thicker gate insulator (1 micron) over the channel near the drain end, the second gate can operate at potentials up to 500 volts.

The polarity of the second gate is chosen so as to enhance the n-layer induced by surface states for an N channel device or to deplete the layer for a P-channel.

For the radiation experiment, a p-channel IGT was exposed to the 31 Mev beam of the University of Southern California proton Linac in a sequence of exposure up to $2 \cdot 5 \times 10^{12}$ protons/cm^2. Curve tracer measure-

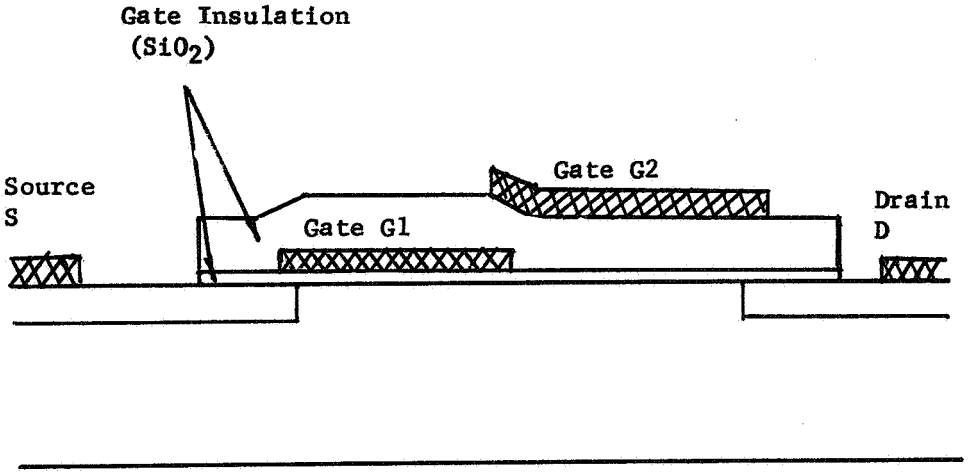

FIGURE A1 - CROSS SECTION OF
INSULATED GATE TETRODE

ments were made of the drain voltage-drain current characteristics at two bias levels, zero and -100 volts. No bias was applied during irradiation. The results are shown in Figure A2, the case for V_{G2}=0 and Figure A3, for V_{G2}=-100 volts. From this data the drain current, as a function of gate voltage, at a constant drain-to-source potential of -80 volts, is shown in Figure A4. It is clear from the curves that the irradiation has shifted the threshold voltage of the device to more negative values. This result in characteristic of the type of radiation effect that occurs in the insulated gate device when exposed to ionizing radiation. Briefly, the radiation causes the production of excess holes and electrons in the silicon dioxide gate material. A separation of this charge occurs with a predominantly positive charge becoming localized in the silicon dioxide at the silicon interface. The presence of this positive charge tends to drive the surface towards accumulation and, consequently, requires a more negative threshold voltage as shown.

In addition to the shift in threshold voltage, it also appears that the breakdown voltage is decreased with increasing radiation. The reason for this is not clear. A further interesting effect can be noticed in the V_{G2}=0 characteristics. With increasing radiation, a square law behavior begins to appear near the origin. This resembles the characteristic observed for devices in which a conducting channel is not present in the region near the drain and the current flowing in the triode region is space charge limited. An explanation for this is the growth of the positive charge in the thicker oxide under the second gate . This tends to deplete this region of holes and sets up the space charge limited operation.

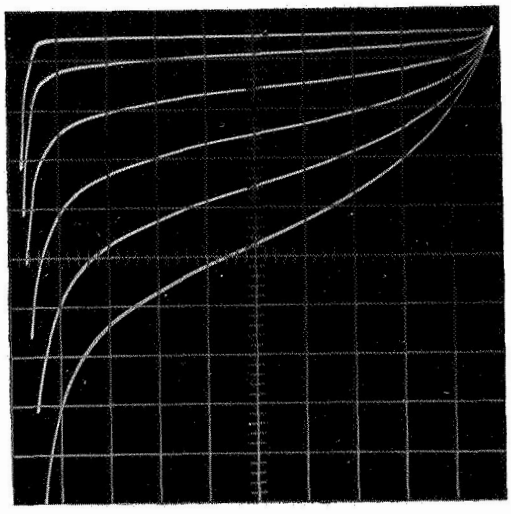

Drain Current	.5 ma/div
Drain Voltage	10 v/div
Initial Step	-8 v
Gate 1	-2v/step
Gate 2	0 volts

A - Pre Irradiation

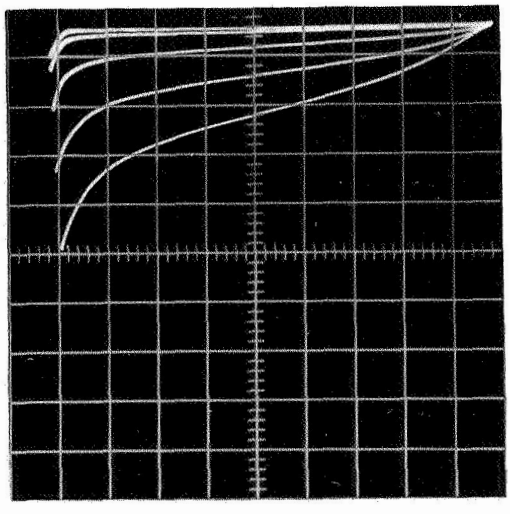

Drain Current	.5 ma/div
Drain Voltage	10 v/div
Initial Step	-12 v
Gate 1	-2v/step
Gate 2	0 volts

B - $\varphi = 2.5 \cdot 10^{12}$ protons/$_{cm}^2$

FIGURE A2 - RADIATION INDUCED CHANGES
IN MOS TETRODE TRANSFER CHARACTERISTICS

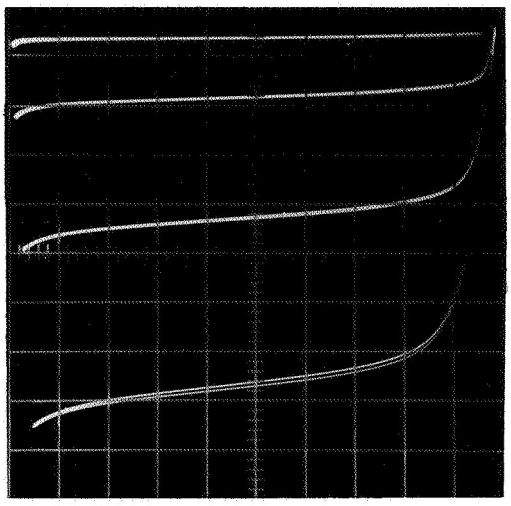

Drain Current	.5 ma/div
Drain Voltage	10 v/div
Initial Step	-8 v
Gate 1	-2 v/step
Gate 2	-100 volts

A - Pre Irradiation

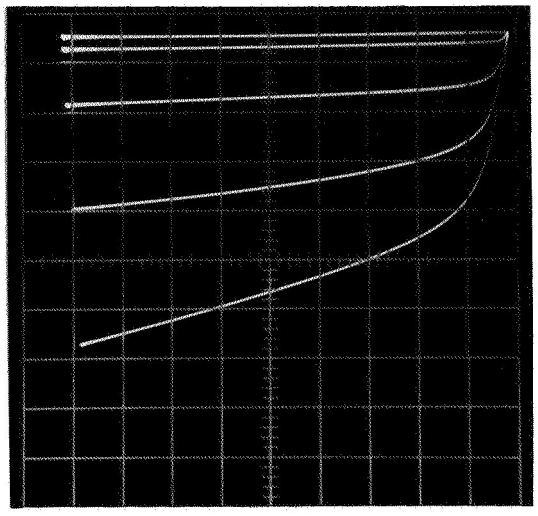

Drain Current	.5 ma/div
Drain Voltage	10 v/div
Initial Step	-12 v
Gate 1	-2 v/step
Gate 2	-100 volts

B - $\varphi = 2.5 \cdot 10^{12}$ protons/cm^2

FIGURE A3 - RADIATION INDUCED CHANGES
IN MOS TETRODE TRANSFER CHARACTERISTICS

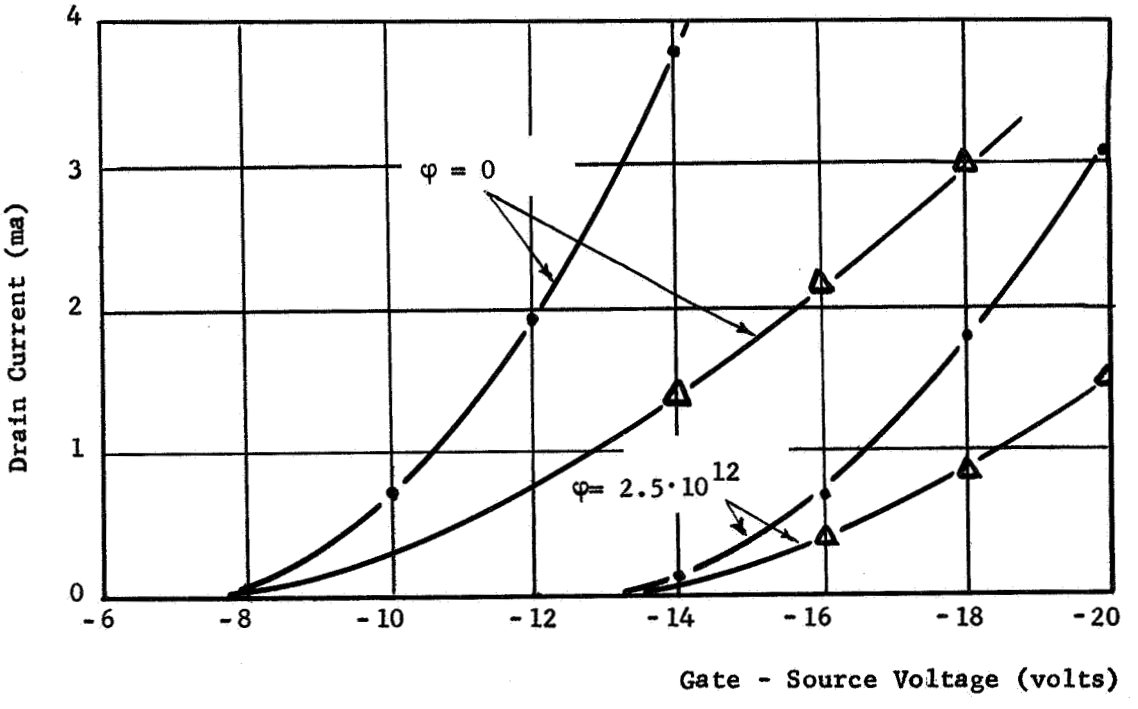

FIGURE A4 - RADIATION INDUCED CHANGES
IN DRAIN CURRENT CHARACTERISTIC

• V_{g2} = 100v

Δ V_{g2} = 0v

ACKNOWLEDGEMENTS

We would like to express our appreciation to Mr. Ray Totah, of the Hughes Newport Devices and Monolithic Circuit Development Department, for his support in fabrication of the transistor design variations and discussion of design effects. We would also like to acknowledge many helpful discussions with Mr. George Wolfe, Associate Department Head. Mr. Harry Sampson assisted in experimental design and instrumentation for data acquisition. We also wish to acknowledge the personal effort of Professor Charles Waddell in making the University of Southern California proton linac available for our use.

REFERENCES

1. Mitchell, J. P.; et al: A Summary of Surface Effects of Radiation on Semiconductor Devices, (AFCRL-65-898, ASTIA No. AD 628 691) Bell Telehpone Laboratory, December 1965.

2. Warner, R. M., Jr.; Fordenwalt, J. N., ed: "Integrated Circuits", McGraw Hill, New York, 1965.

3. Honnold, V. R.; Thomas, G. D.; Berggren, C. C.; Transistor Design Effects on Radiation Resistance, NASA CR-590, September 1966.

4. Messenger, G. C.: Nuclear Radiation Effects Conference, IEEE PGNS, Seattle, Washington, July 1964.

5. Philips, A. B.: "Transistor Engineering", McGraw Hill, New York, 1962.

6. Philips, A. B.: op. cit. page 185.

7. Klein, M.: Proceedings of the IRE, November 1961, Page 1708.

8. Curtis, O. L. Jr.; Germano, C. A.: IEEE Transactions on Nuclear Science, Vol. NS-14, December 1967, Page 68.

9. Volk, W.: "Applied Statistics for Engineers", McGraw Hill, New York, 1958, Chapter 7.

10. Johnson, N. L.; Leave, F. C.; "Statistics and Experimental Design", V 2, John Wiley and Sons, Inc., 1964.

11. H. G. Dill, Proc. IEEE 54, 1494 (1966)

REFERENCES (continued)

12. H. G. Dill, "Offset Gate Field Effect Transistors with High Drain Breakdown Potential and Low Miller Feedback Capacitance", Dissertation, Swiss Federal Institute of Technology, Zurich, 1967.

NASA-Langley, 1968 —— 10

"The aeronautical and space activities of the United States shall be conducted so as to contribute . . . to the expansion of human knowledge of phenomena in the atmosphere and space. The Administration shall provide for the widest practicable and appropriate dissemination of information concerning its activities and the results thereof."

— NATIONAL AERONAUTICS AND SPACE ACT OF 1958

NASA SCIENTIFIC AND TECHNICAL PUBLICATIONS

TECHNICAL REPORTS: Scientific and technical information considered important, complete, and a lasting contribution to existing knowledge.

TECHNICAL NOTES: Information less broad in scope but nevertheless of importance as a contribution to existing knowledge.

TECHNICAL MEMORANDUMS: Information receiving limited distribution because of preliminary data, security classification, or other reasons.

CONTRACTOR REPORTS: Scientific and technical information generated under a NASA contract or grant and considered an important contribution to existing knowledge.

TECHNICAL TRANSLATIONS: Information published in a foreign language considered to merit NASA distribution in English.

SPECIAL PUBLICATIONS: Information derived from or of value to NASA activities. Publications include conference proceedings, monographs, data compilations, handbooks, sourcebooks, and special bibliographies.

TECHNOLOGY UTILIZATION PUBLICATIONS: Information on technology used by NASA that may be of particular interest in commercial and other non-aerospace applications. Publications include Tech Briefs, Technology Utilization Reports and Notes, and Technology Surveys.

Details on the availability of these publications may be obtained from:

SCIENTIFIC AND TECHNICAL INFORMATION DIVISION

NATIONAL AERONAUTICS AND SPACE ADMINISTRATION

Washington, D.C. 20546